Future microfluidic and nanofluidic modular platforms for nucleic acid liquid biopsy in precision medicine

Ana Egatz-Gomez,[1] Ceming Wang,[1] Flora Klacsmann,[1] Zehao Pan,[1] Steve Marczak,[1] Yunshan Wang,[2] Gongchen Sun,[1] Satyajyoti Senapati,[1] and Hsueh-Chia Chang[1,a)]

[1]*Center for Microfluidics and Medical Diagnostics, Department of Chemical and Biomolecular Engineering, University of Notre Dame, Notre Dame, Indiana 46556, USA*
[2]*Electrical and Computer Engineering, University of Utah, Salt Lake City, Utah 84112, USA*

(Received 8 February 2016; accepted 20 April 2016; published online 5 May 2016)

Nucleic acid biomarkers have enormous potential in non-invasive diagnostics and disease management. In medical research and in the near future in the clinics, there is a great demand for accurate miRNA, mRNA, and ctDNA identification and profiling. They may lead to screening of early stage cancer that is not detectable by tissue biopsy or imaging. Moreover, because their cost is low and they are non-invasive, they can become a regular screening test during annual checkups or allow a dynamic treatment program that adjusts its drug and dosage frequently. We briefly review a few existing viral and endogenous RNA assays that have been approved by the Federal Drug Administration. These tests are based on the main nucleic acid detection technologies, namely, quantitative reverse transcription polymerase chain reaction (PCR), microarrays, and next-generation sequencing. Several of the challenges that these three technologies still face regarding the quantitative measurement of a panel of nucleic acids are outlined. Finally, we review a cluster of microfluidic technologies from our group with potential for point-of-care nucleic acid quantification without nucleic acid amplification, designed to overcome specific limitations of current technologies. We suggest that integration of these technologies in a modular design can offer a low-cost, robust, and yet sensitive/selective platform for a variety of precision medicine applications. *Published by AIP Publishing.* [http://dx.doi.org/10.1063/1.4948525]

I. INTRODUCTION

Nucleic acid biomarkers, including messenger RNA (mRNA), micro RNA (miRNA), and circulating tumor DNA (ctDNA), have enormous potential in diagnostics and management of cancer and other diseases. Coding and non-coding RNA influence gene expression and regulation and can have varying expression levels across various pathological conditions including cancer, autoimmune and inflammatory diseases, and cardiovascular diseases.[1–3] An important advantage of RNA is that it allows the identification of transcriptionally active viruses and genes. Micro RNA and their counterpart small interfering RNA (siRNA)[4] are short (18–22 nucleotides long) non-coding and regulatory RNAs, particularly resistant to degradation in blood, whose expression level has been connected to specific diseases. In addition to transcription products, cancer cells release DNA (ctDNA) in different forms and levels into the blood of cancer patients. Quantitative detection ctDNA holds promise for early detection of specific cancers, assessment of the tumor size, and prognosis under a specific chemotherapy.[5]

There is a great interest for accurate miRNA, mRNA, siRNA, and ctDNA identification and profiling—quantification of a panel of these nucleic acid markers. But to date, no technology can perform this very challenging task with precision, ease, low cost, and high throughput. All three main technologies, quantitative reverse transcription polymerase chain reaction

a)Author to whom correspondence should be addressed. Electronic mail: hchang@nd.edu.

(qRT-PCR), microarray hybridization, and next-generation sequencing (NGS), face challenges in nucleic acid profiling. Equipment and analysis costs, throughput, and normalization[6,7] still represent obstacles for large-scale nucleic acid biomarker validation[8–14] and adoption in the clinics[15–17] Differences in the nucleic acid purification method, detection technology, and laboratory protocol often lead to different profiling results. Consequently, interpretation of differential expression data and comparisons across different studies has to be done with a note of caution, as standard deviations can span several orders of magnitude.[18,19] Such statistical errors are particularly worrisome for down-regulated and low copy number targets. There are many reasons for these variations, including analyte loss due to the extraction method, long assay times that exacerbate nucleic acid degradation, different PCR amplification rates, probe saturation in microarrays by non-targets particularly for long binding sequences, when hybridization thermodynamics is not selective, etc.[20–22]

It is our belief that micro- and nano-fluidics, when properly integrated and applied, can lead to a simple, easy to use, sensitive and selective nucleic acid profiling platform, capable of counting specific native miRNAs, mRNAs and circulating tumor DNA (ctDNA) at low copy numbers, in less than one hour (although more stable than RNAs, miRNAs still degrade over time), with little loss due to transfer and handling, with neither PCR amplification or off-chip extraction/preservation, for future personalized/precision medicine. Such point-of-care (POC) technology would offer low-cost liquid biopsy (e.g., detection of nucleic acids shed into the blood from primary tumors and from metastatic sites), screening, and prognosis tests for dynamic adjustment of therapeutic agent dosage and composition. The prognosis potential is particularly intriguing and will probably be realized before the diagnosis applications since some target nucleic acids for prognosis are already known, which reduces the multiplex complexity.

Quantitative and ultra-sensitive measurement of ctDNA, mRNA, and miRNAs can be used for patient management, especially in conjunction with promising upcoming RNA-targeting therapies that require precise measurement of RNA-mimicking therapeutic agents and/or RNA and small RNA drug targets. For example, in the Federal Drug Administration (FDA) orphan drug product designation database, we found about 20 orphan-designated, not yet approved, RNA-targeting drugs from several different for treatment of diseases such as muscular dystrophy, cancer, hemophilia, and fibrosis cystic.[23] Using the keywords RNA, mRNA, micro-RNA, or mi-RNA in ClinicalTrials.gov, we found more than 1800 currently open studies as of January of 2016, of which 188 are focused on miRNAs. The majority of these 188 studies are aimed at miRNA biomarker assessment in disease diagnostics and monitoring, and two of them deal with evaluation of miRNA-mimicking drugs in hematological malignancies and pathological fibrosis and Hepatitis C. A detailed review of pre-clinical and clinical trials involving RNA-targeting drugs has been recently published.[24]

In view of the upcoming need for precise, quantitative detection for measurement of nucleic acid biomarkers for diagnosis and patient therapy management, we will first briefly review commercially available detection/quantification technologies for RNA species and viral RNA. Second, we review the analytical limitations of the three mainstream technologies for multiplex quantitative detection of nucleic acids. Finally, we summarize our most recent efforts on microfluidic and nanofluidic technology development, suggest how these technologies may help overcome the current limitations of the mainstream technologies, and propose that proper integration of several microfluidics and nanofluidics components can offer such a requisite nucleic acid profiling platform for future genomic medicine applications.

II. FDA-APPROVED RNA ASSAYS AND PLATFORMS

The two more mature areas in RNA-based detection are virus and cancer diagnostics. In recent years, FDA has approved several platforms and assays,[25] some of which are summarized in Table I.

Viral assays are important in the diagnosis of infectious disease and the management of virus-induced cancers. With the advent of novel antiviral therapies for human

TABLE I. Summary of FDA-approved nucleic-acid assays and platforms.

Assay	Platform	Target	Tissue	Application	Ref.
Veridex	RT-PCR	mRNA	Formalin-fixed, paraffin-embedded tissue	Cancer of unknown primary origin	37
miRview (Rosetta genomics)	Microarray	miRNA	Formalin-fixed, paraffin-embedded tissue	Cancer of unknown primary origin	37
Cancer Type ID (Biotheragnostics)	Taqman™-RT-PCR	mRNA	Formalin-fixed, paraffin-embedded tissue	Cancer of unknown primary origin	37
CupPrint	Microarray	miRNA	Formalin-fixed, paraffin-embedded tissue	Cancer of unknown primary origin	37
Genesearch (Veridex)	RT-PCR	mRNA	Lymph node tissue	Breast cancer metastasis	38–40
mi-LUNG (Rosetta genomics)	Microarray	miRNA	Fine needle aspiration; bronchial brushing	Lung cancer type	41
Reveal (Rosetta genomics)	Microarray	miRNA	Fine needle aspiration	Thyroid cancer stratification	42
mi-KIDNEY (Rosetta genomics)	Microarray	miRNA		Kidney cancer type	43
Prosigna nCounter (Nanostring)	Signal amplification (hybridization)	mRNA	FFPE	Breast cancer recurrence	44 and 45
Versant (Siemens)	RT- PCR; signal amplification	Viral RNA	Serum	HCV, HIV-1	28
RealTime (Abbot),	Real-time RT-PCR	Viral RNA	Serum	HCV, HIV-1	26 and 29
Procleix (GenProbe),	Real-time RT-PCR	Viral RNA	Serum	HCV, HIV-1	30
Cobbas (Roche)	Real-time RT-PCR	Viral RNA	Serum	HCV,HIV-1	26 and 29
Aptima (Hologic)	Isothermal quantitative RT-PCR; Tigris® DTS® and Panther®	Viral RNA, E6/E7 transcripts from high-risk HPV genotypes	Serum, cervical cytology	HCV, HIV-1, HPV	31 and 32
NucliSENS /NorChip (BioMérieux)	Nucleic acid sequence–based amplification (NASBA)	Viral RNA, E6/E7 mRNA from high risk HPV types	Throat swabs, cerebrospinal fluid (enterovirus); uterine cervical cytology specimens (HPV)	Enterovirus, HPV	33 and 34

immunodeficiency virus (HIV) and hepatitis C virus (HCV), assays for virus quantification with high sensitivity are becoming increasingly important for optimal patient management.[26] The gold standards for viral infection detection have traditionally been viral culture, where host cells are cultured to detect structural changes caused by viral invasion, and immunoassays for detection of antigens and antibodies to viral proteins. These methods are expensive and time-consuming, require designated laboratories, and cannot always identify the viral serotype. Viruses can be also detected using viral genomic DNA and genomic, messenger and micro RNA.[27] Recently, FDA has approved several assays and platforms for detection of genomic and messenger viral RNA, summarized in Table I.[26,28–34] These platforms offer a limit of detection (LOD) of 10–200 copies/ml, and linear quantification up to 10^{-8} copies/ml. Such new point-of care diagnostic assays capable of achieving comparable or lower limits of detection than current ones would allow better patient management with antiviral therapies and maybe even allow higher cure rates.[35] The technologies for viral-RNA diagnostics may eventually be approved for other RNA-based diagnostic applications.

In cancer diagnosis, the gold standard remains the histological examination of affected tissue, obtained either by surgical excision, or radiologically guided biopsy. Such procedures are expensive, not without risk to the patient, and require consistent evaluation by expert pathologists. In cancer, the transcriptome offers the opportunity to analyze genes that are being actively expressed.[36] A handful of miRNA-based tests aimed at guiding therapeutic management have been already approved by FDA for applications such as classification of cancer of unknown primary origin (CUP), lung cancer type classification, thyroid cancer stratification, and breast cancer metastasis and recurrence analysis, based on the differential expression of miRNA biomarker sets.[37–45] Unlike the tests for viral RNA, which are offered as kits with a companion platform, cancer testing is offered as a service to healthcare providers. Most studies so far have dealt measuring the concordance of test results with immunohistochemistry and pathology in cancer typing and stratification. Although results show that in some areas molecular expression profiling may be used to guide decisions regarding treatment and improve patient outcomes, this field is in its very early infancy and adoption by the clinical practice needs many more clinical studies to come.[46]

III. CHALLENGES FACED BY THE MAIN TECHNOLOGIES IN NUCLEIC ACID ANALYSIS

The four mainstream technologies for nucleic acid analysis are Southern and Northern Blotting, PCR, microarrays, and next-generation sequencing. Blotting involves electrophoretic separation of nucleic acids in a gel, transfer of the separated components to a membrane, and detection of specific sequences by probing the membrane. This technique has been superseded by PCR in many applications because it is labor-intensive, it has low sensitivity, and it requires large amount of starting material.

In qRT-PCR, the starting material is total RNA or messenger RNA (mRNA). RNA is first transcribed into complementary DNA (cDNA) by a reverse transcriptase enzyme. Transcription is followed by many cycles of PCR, in which another enzyme, DNA polymerase, synthesizes DNA strands using a specific section of the cDNA as a template (extension), followed by a denaturation step where the newly synthesized strand is separated from the template at high temperature. In every cycle, the number of DNA strands is doubled, leading to an exponential amplification of targets. In quantitative PCR, DNA is fluorescently labeled, and the amount of the fluorescence released during amplification is directly proportional to the amount of amplified DNA. If a sample contains more cDNA targets, the fluorescence will be detected in an earlier quantitation cycle (Cq). Typically, qPCR dynamic range is 10^2–10^7 copies of an individual cDNA.[47]

DNA microarrays consist of an ordered arrangement of thousands of identified sequenced genes attached to a solid support. Each identified sequenced gene corresponds to a fragment of genomic DNA, cDNAs, PCR products, or chemically synthetic oligonucleotides, up to 70 mers. Although not typically used for absolute but for relative quantitation in miRNA expression studies, it can be estimated that microarrays have a linear range of 10^6–10^{10} copies of an individual cDNA.[48]

The most widely used sequencing method, Sanger sequencing, uses standard nucleobases along with modified nucleobases in parallel PCR reactions. When a modified nucleobase is incorporated by the polymerase, DNA duplication is terminated. The sequence is obtained by analysis of the amplification products with different lengths by gel electrophoresis. The first human genome, published in 2001, took 15 years to sequence, and cost about 3 billion dollars. In next-generation sequencing, this principle is extended across millions of fragments in a massively parallel fashion. Today's next generation sequencing (NGS) systems are capable of sequencing several human genomes in one day, at a cost of $1000 each.[49] NGS sequencing offers a much larger dynamic range than PCR. It is also possible to detect long nucleic acids without previous knowledge of their sequences, however, de novo sequencing of short nucleic acids is still limited by the relatively high rate of NGS errors. The main disadvantage of NGS in a clinical setting is putting in place the required infrastructure, computer capacity, and personnel expertise to run the experiments and comprehensively interpret data.

Because of cost, pretreatment, throughput, normalization and sensitivity issues, none of the above-mentioned techniques can be readily converted to POC platforms.[8–17,50–55] Reliable quantification of mRNA and microRNA levels for diagnostic and prognostic purposes requires optimal RNA quality and quantity. However, the different instances along the RNA and miRNA analysis workflow can lead to length, sequence, and structure-specific biases in the final expression analysis of a given set of small RNAs. The correlation of small RNA measurements to the original RNA abundance in a sample thus can be variable. Reported miRNA up/down regulation using different technologies and protocols is often inconsistent; with standard deviations often over 1 or 2 decades.[56–59] In Secs. III A–III G, we outline the associated challenges associated with accurate RNA and ctDNA quantitation. A comparison of commercial systems based on these main technologies can be found in a number of recent reviews.[21,60]

A. RNA extraction and purification

The results of gene expression analysis are directly affected by RNA extraction, which can greatly affect mRNA and miRNA quantity and integrity. Extraction is necessary since the sample may contain nucleases that degrade RNA, variability of the sample pH may affect PCR cycling efficiency, and cross-hybridization of the majority non-targets can affect the sensitivity/selectivity of surface assays such as microarrays. Unfortunately, the efficiency of extraction methods is highly protocol- and sample- sensitive. There is no consensus about the best extraction method. There are optimized protocols for different types of samples, such as blood,[61–63] circulating RNA and other biological fluids,[64–66] microvesicles,[67–69] frozen tissue, formalin-fixed tissue,[70] with three general approaches. Methods that rely on the different solubility of DNA, RNA, proteins, and other cellular components in different organic solvents (phenol: chloroform method) are the gold standard for customized in-lab protocols. Their main drawbacks are that they are prone to cross-contamination between the phases, RNA degradation, incomplete separation from proteins, and loss of the small RNAs. Methods based on the ability of RNA to adsorb on specific surfaces in presence of chaotropic salts such as beads or test tubes are used in many commercially available kits; however, some of these protocols are complex and have to be carefully performed to avoid sample loss. Finally, equilibrium gradient centrifugation is a labor-intensive approach, often the method of choice for the purest RNA fractions. RNA extraction methods and commercially available kits have been reviewed in detail recently.[71]

Separation of messenger RNA (mRNA) requires special considerations. It constitutes 1%–5% of the total RNA. Messenger RNA can be purified from total RNA, or directly from the intact sample. Eukaryotic mRNA features a polyadenylate tail, which is used to capture mRNA using complementary probes covalently bound to special matrices or beads. Ideally, the purified mRNA should be free from other RNAs such as transfer and ribosomal RNA. Even more challenging is the extraction of miRNAs. They represent only a small fraction ($\sim$0.01%) of the mass of a total RNA sample.[72] The low abundance and short length of miRNAs places very stringent yield, integrity and purification requirements on extraction methods, which can introduce sequence-specific biases in profiling results.[66,73–75] In general, small RNAs have a

better chance to be purified directly for a sample using specific kits than from using organic-phase extracted total RNA.[64,76]

B. RNA end-modification

The same as all DNA polymerases, RNA transcriptases can only add new nucleotides to an existing DNA strand, therefore, they require a primer (i.e., a short strand about 10 bases long complementary to the initial section of the template) to initiate the synthesis of cDNA. Due to their small length and the absence of a common sequence that can be used for identification and primer design, the analysis of non-coding small RNAs with qRT-PCR, microarrays, and sequencing, typically requires RNA end-enzymatic modification prior to transcription into cDNA. Assays typically involve steps such as adapter ligation, poly(A) tailing, and ligase- and polymerase-based fluorescent labeling of RNA. These reactions have inherent sequence-specific biases because the enzymes involved are sensitive to varying degrees to the sequence and structure of their nucleic acid substrates. These biases can be present and even can be amplified in the final relative concentration analysis by the three main techniques, microarrays, qRT-PCR, and sequencing.[77–79]

C. Detection of point mutations and polymorphisms

Variations in miRNA and sequence, even of a single nucleotide, can potentially affect the regulation of multiple genes and pathways.[80] MicroRNAs exist in families in which members vary by as little as a single nucleotide, placing ultra-high sensitivity and specificity requirements on systems for detection of miRNAs. The short length and sequence similarity present obstacles for primer or probe design and hybridization in microarrays or qPCR.[21] Specificity of a probe (in microarray or signal amplification systems) or primer (in target amplification systems) for its target can be boosted with high temperatures, so that only the best match binds. However, microRNAs vary greatly in their percentage of guanines and cytosines (GC content). This implies melting temperatures can vary by more than 20 °C, complicating the design of assays that depend on melting and re-annealing of complementary sequences such as PCR. Among the established technologies, NGS is the technology that can best differentiate between miRNA isoforms, however, sequence similarity of miRNAs may still cause problems in discriminating between miRNAs due to amplification steps and sequencing errors.[81]

D. Quantitative reverse transcription-PCR (qRT-PCR)

qRT-PCR can provide a very high sensitivity and specificity at a medium cost. It requires relatively low amounts of RNA, and it can perform absolute quantification. However, due to the short 20-base length of miRNAs, selectivity is a major issue both during reverse transcription and PCR unless end modification discussed above is implemented. Target loss during these additional steps limits it to significantly over-expressed miRNAs and to a very low throughput of only a handful of samples per day. Nevertheless, qRT-PCR has become the standard for the detection and quantification of longer RNA targets. It starts with the conversion of RNA into a cDNA template by an RNA-dependent DNA polymerase (reverse transcriptase) followed by quantitative PCR (qPCR). The transcription step is an important source of variability, as reverse transcriptases efficiency can be sequence, length, and structure dependent. In multiplex qRT-PCR amplification, biases can be introduced by varying GC content, length, starting concentration of the cDNAs, and even by buffer composition.[79,82–84] As a result, often PCR cycle numbers (Cq) distributions are skewed relative to actual miRNA copy numbers, even with the latest locked nucleic acid (LNA) technology.[85–93] The same multiplex qRT-PCR test can have limits of detection that are different by several orders of magnitude for different virus serotypes.[94,95] The problem of discordant results between different platforms becomes worse in the case of low viral loads.[96] Nested qRT-PCR can increase detection sensitivity; however, it is more sensitive to contamination and has higher false-positive rates.[97] Droplet digital PCR was recently suggested as a minimal sample preparation substitute for qRT-PCR; but it remains highly equipment/personnel intensive.[98,99]

E. Microarrays

This is the technology with the lowest cost and higher throughput with respect to the number of samples that can be processed per day. However, microarrays have a lower specificity, sensitivity, and dynamic range than qRT-PCR or RNA sequencing, cannot be used for miRNAs with unknown sequence, and do not provide a direct quantitative measurement[92] The short length of miRNAs limits the options for designing complementary probes often making necessary to use the entire microRNA sequence. As in qRT-PCR, makes it difficult to find unique experimental conditions and strategies that work well with a given population of miRNAs that may be very similar in sequence. Before hybridization miRNAs are usually end-modified with fluorescent tags and adapters and amplified by PCR, which are processes prone to concentration and sequence-dependent biases as discussed previously. Thermodynamic equilibrium is critical in heterogeneous DNA hybridization assays. Considerable cross-hybridization occurs and quite often the hybridization thermodynamics is not sufficiently selective. Targets at lower concentrations require longer assay (transport) times to be measured with the same accuracy as those that are up regulated. Such long assay times enhance non-specific binding of the target, as non-targets with large copy numbers can saturate probes. Systematic hybridization bias is frequently found when hybridization reactions are not driven to completion.[100] In general, intra- and inter-platform reproducibility is low, even using locked nucleic acid (LNA) probes. Lower reproducibility stipulates a large number of replicates, raising costs, and experimental complexity.[7]

F. Next generation sequencing

Despite being the most expensive technology of the three, high-throughput sequencing of miRNAs is becoming the dominant technology in the discovery and experimental validation of novel or predicted miRNAs. It can discriminate between very similar miRNAs. The process starts with the reverse transcription of a cDNA library from the RNA-containing as in qRT-PCR. Adaptors are ligated to the ends of the cDNA, and the resulting products are attached to a substrate. Massively parallel sequencing is performed on the millions of individual cDNA molecules from the library. After bioinformatic processing, the sequence reads are then aligned against a miRNA sequence database to identify the known and unknown miRNAs present in the sample. These data also provide quantification by identifying the number of sequence reads. The main disadvantage of NGS in regards to quantification is that NGS faces the same biases due to enzyme processing of the miRNAs as qRT-PCR and microarrays, which can end up in a systematic misrepresentation of the miRNA complement.[7,81] In addition, sequencing remains too costly even with emerging protein-nanopore sequencing technologies.[57,101]

G. Digital PCR

The most developed, however, not yet approved by FDA, technology for ctDNA and miRNA profiling is digital droplet PCR. This method reduces the error due to variation in amplification efficiency, as miRNA molecules are counted one at a time. However, digital PCR still suffers from several disadvantages.[102–104] The copy numbers of different targets in a sample are often not known a priori and can vary by several orders of magnitude. Digital PCR quantification is most accurate at very low copy numbers, when estimates by Poisson statistics are not necessary. Thus, different targets have to be diluted proportionally to their concentration in the sample, which calls for very large sample volumes for multi-target profiling, and in the case of unknown copies of targets, repetitive dilution. Finally, for accurate absolute quantification of the amplified target, the droplets (10–100 μm in size) need to be in a single file to be interrogated individually in flow-cytometry fashion, because in an emulsion of aqueous droplets in oil scattering is highly dependent on the position of the droplets. The current droplet generation rate in microfluidic chips ($\sim$80 000 drops per second) is not high enough to allow fast analysis of a highly diluted sample. The need for repeated dilution and low throughput are obstacles that need to be overcome before multiplex profiling digital PCR can be done with reasonable sample volumes and assay times.

IV. ALTERNATIVE MICROFLUIDIC AND NANOFLUIDIC PROFILING TECHNOLOGIES

Several emerging technologies have been proposed for analysis of nucleic acids in the nanoscale, seeking to overcome some of the challenges posed by short oligonucleotide detection. These technologies include methods based on rolling-circle isothermal amplification within hydrogel microparticles to compartmentalize multiple reactions,[105] free-solution electrophoretic detection with drag-tags and single stranded DNA binding protein to increase the differences in electrophoretic mobility of target-probe complexes,[106,107] and other biosensor-based approaches, which have been the focus of several recent reviews.[108,109]

In this article, we examine a cluster of microfluidic technologies from our group with potential for POC nucleic acid quantification without PCR amplification, thus eliminating the normalization and selectivity issues of PCR. Without PCR amplification, sensitivity now becomes a challenge, along with other pretreatment related issues. We suggest that integration of these microfluidic technologies can overcome these obstacles and offer a robust platform for the requisite liquid biopsies in precision medicine. Each of them has been designed to overcome specific shortcomings of the nucleic acid diagnostic technologies described in Secs. III A–III G, including sensitivity.

A. Ionic-membrane integrated platform

Our ionic-membrane modular biochip platform currently allows rapid (30–60 min), sensitive and selective quantification of up to three specific miRNAs with an LOD of 10^6 copies, from a small volume of raw cell media or lysate. The dynamic range corresponds to 16–30 cycles of qRT-PCR. This platform is robust against large variations in sample ionic strength and pH, thus eliminating the need for specific protocols. Figure 1 shows our biochip, which integrates modules for extraction of nucleic acids; separation of short miRNAs from cell debris, protein and long RNAs; and capture of specific miRNAs. An on-chip miniaturized gel membrane module is used for removal of cell debris (Fig. 1(a)). A module that concentrates nucleic acids at a spot by ionic-strength depletion action of a membrane follows.[110,111] This concentration action not only reduces assay time but also shifts the thermodynamics in favor of low-copy numbers. Finally, a probe-functionalized solid-state membrane performs yet another target extraction step with much higher selectivity and is used for quantitative sensing. The membrane sensor, rather than the pretreatment and concentration units, is what determines the LOD.

Figure 1(b) shows a picture of our polycarbonate biochip. A micropump sustains a continuous flow through a single microchannel $\sim$1 mm in height and width, at a high rate ($>\mu$l/min) to further reduce adsorption and allow fast transport of analytes along the biochip. As in blood microcirculation, the microchannel in the control unit serves as a clog-free passive transport vehicle without any fabricated electrodes within the channel. Instead, molecules are inserted, trapped, and released along the channel by membrane units, which are precisely controlled by electrodes housed in membrane-separated external reservoirs. The membranes are sub-mm commercial polymer cation- and anion- selective membranes. Membranes and electrode reservoirs are vertically inserted into the microchannel at the biochip pretreatment, preconcentration and probe capture modules through orifices or micro-tips/salt bridges. The biochip exploits different ionic current features of the membranes such as external ion depletion and sensitivity of the overlimiting current to surface bound counter-ions.

1. On-chip miRNA isolation from other nucleic acids

In our biochip, high selectivity and sensitivity is achieved by separating the target molecules from all the other nucleic acids without significant loss. The sample is loaded into the reservoir at the pretreatment unit (Fig. 1(a)). The lysing solution ensures most proteins, and in particular, inhibitors such as hemoglobin and immunoglobin G, remain in the organic phase while RNA molecules separate out in the aqueous phase. All negatively charged molecules are later stacked at the membrane surface by isotachophoresis using a pulsed current. A short high-intensity pulse then propels short miRNAs across the membrane, leaving behind the much longer ($\sim$kb) and more numerous (by six orders of magnitude) genomic DNA. Figure 2 shows gel

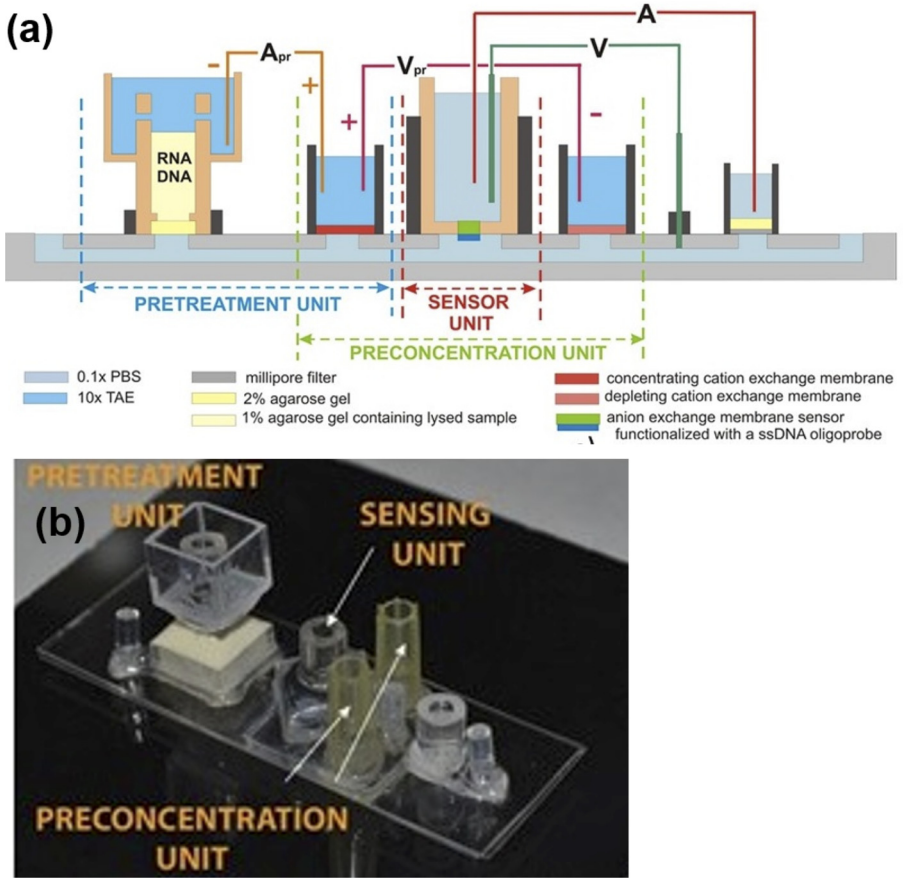

FIG. 1. Integrated biochip. (a) Pretreatment Unit for nucleic acid extraction from lysed cells. (b) Integrated chip picture. Inset: heterogeneous commercial polymer membrane SEM. Adapted with permission from Slouka *et al.*, Talanta **145**, 35–42 (2015). Copyright 2015 Elsevier.[182]

electrophoresis analysis of *E. coli* lysate purified with our pretreatment unit and with a commercial kit. Cell debris, all proteins (Fig. 2(a)) and nucleic acids longer than 200 bases (Fig. 2(b)) are essentially removed by our pretreatment unit, while significant amounts of short RNAs(∼100nt) remain in the effluent (Fig. 2(c)).

In the experiments shown in Figure 2, we estimate that 10^8–10^{14} short (∼100 bases-long) nucleic acids were isolated from the raw sample. Using our membrane sensor 10^6–10^{10} copies of a specific nucleic acid within this population can be quantified in one hour. In the remaining sections of this article, we shall propose some additional modules that may be used to cover the remaining 10^2–10^5, without PCR amplification.

2. On-chip low-loss analyte preconcentration

The preconcentration step allows us to achieve both rapidity and sensitivity and minimize target loss. To reduce the long diffusion-limited assay time (hours), high-Peclet (Pe) number (∼1000) convection is used to transport analytes to the sensor in the microchannel. However, the rapidity of high-Pe microfluidic flow can also cause dispersion and analyte loss. To offset this trade-off, we use an ion-depletion strategy to concentrate targets at the sensor. A cation-selective membrane is placed on the microchannel downstream from the sensor. A negative voltage is applied to the cation-selective membrane to create an ion-depleted region with a high electric field. Much like isotachophoresis,[112] due to the discontinuity of the electric field, charged molecules concentrate at the boundary of the depletion region without the need of using different buffers. The short nucleic acids from the pretreatment module can be rapidly concentrated in a millimeter-sized band at the

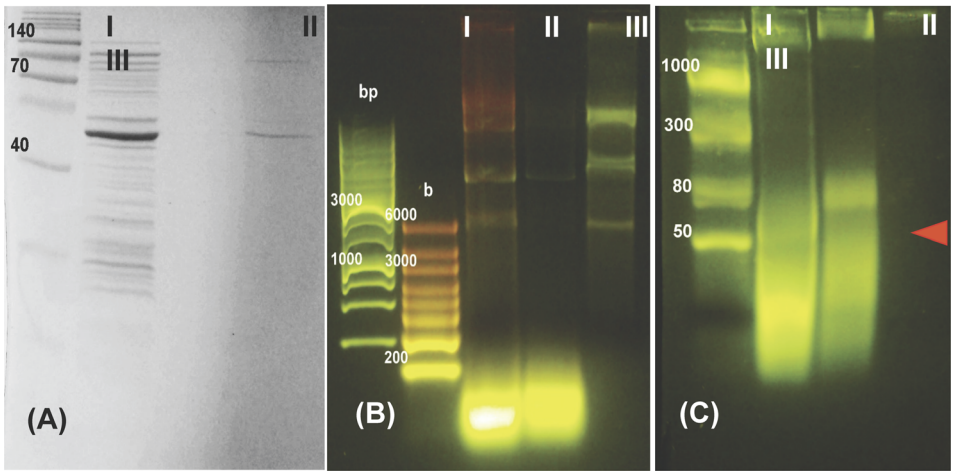

FIG. 2. Pre-pretreatment unit sample analysis. Lane I, *E. Coli* lysate before loading; lane II, sample after pretreatment unit; lane III, *E. coli* lysate purified with Qiagen total RNA purification kit. (a) Total protein profile of the samples characterized by acrylamide gel electrophoresis (SDS-PAGE). An aliquot of each sample were electrophoresed in 12% gel and the protein bands were visualized with Coomassie stain. No protein bands are discernible in the output of our pretreatment unit. (b) Long nucleic acids were characterized on 1% Agarose gel with MOPS buffer (ran on 100 V for 60 min). Most long nucleic acids in the sample are removed at the output of our pretreatment unit. (c) Short nucleic acids were characterized on a 3% agarose gel with sodium boric acid buffer, ran for 10 min at 300 V. The red arrow is likely a transfer-RNA band in the output from our pretreatment unit. Most short nucleic acids present in the original sample have been recovered after our pretreatment unit. Our unit appears to perform significantly better that the commercial kit in our hands.

sensor (Figs. 1(a) and 1(b)). From fluorescent measurements, we estimate that despite the robust flow, nucleic acids are concentrated by a factor of 200 with no more than 1% analyte loss.[111] Since the hydrodynamic and electrophoretic mobilities of nucleic acids are size sensitive, by imposing pressure-driven flow onto the concentrated band, larger molecules are separated by flow-isotachophoresis. An additional advantage to introducing pressure-driven flow is that, as shear is an irreversible process unencumbered by thermodynamics, the washing action of the high shear-rate flow across the probe-based capture unit can enhance selectivity beyond what is permitted by adsorption isotherm for non-targets, making possible efficient removal of non-specifically bound non-targets and single-mismatch discrimination.[113]

3. Probe-based capture robustness against sample pH and ionic strength

A further advantage to our ionic-membrane concentration and detection units is their robustness to sample pH and salt concentration variations. The membrane action essentially establishes de-ionized water condition at the depletion region.[110,111] The same is true for the probe-based capture module. The depletion action of ion-selective membrane still occurs when the main channel is filled with gel, which allows improving the separation and concentration of the nucleic acids in the gel without bulk flow.

Target-specific probes are covalently immobilized on the ionic-membrane surface facing the sensing reservoir (Fig. 3(a)). This membrane has a permanent positive charge and very narrow pores, so it permits the passage of small negative ions, but does not allow transit of target molecules. The membrane ion depletion action expands the equilibrium Debye layer into an extended space charge region by osmotic pressure and induces surface microvortex instabilities.[111,114] Mixing due to these vortices results in an overlimiting current and an inflection point in the current-voltage (I-V) curve (Fig. 3(b)). After probe functionalization, and also upon target hybridization with membrane-bound probes, surface charge inversion reduces the membrane ion-conductance and produces a large shift (hundreds of millivolts) in the I-V characteristic curves, which correlates to the number of captured target molecules (Fig. 3(b)).[114] The large shift is the result of hybridized target molecules reducing the membrane depletion action, the space charge thickness, and the microvortices intensity. This phenomenon can be

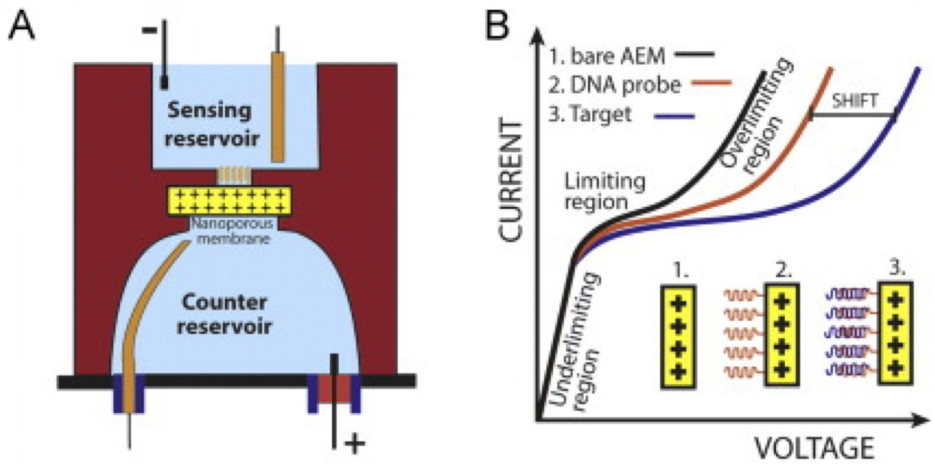

FIG. 3. Ionic-membrane sensor. (a) Schematic showing the ionic-membrane membrane between a sensing and counter reservoirs. Capture probes are functionalized on the side of the membrane facing the sensing reservoir. (b) Schematics of the characteristic I-V curves of a membrane without any probe (AEM: anion-exchange membrane; black line), with a functionalized probe (red line), and after target hybridization with the probe (blue line). The shift of the I-V curves can be correlated to the number of target molecules present in the sample. Adapted with permission from Senapati *et al*., Biomicrofluidics **60**, 92–100 (2014). Copyright 2014 AIP Publishing.[118]

mathematically attributed to the inflection point of the *I-V* curve at the onset of the overlimiting current.[111,114] The high local electric field, shear from the microfluidic flow, and shear due to the mixing vortices further minimizes non-specific adsorption[113,115] and can be used to linearize miRNA hairpins to facilitate probe hybridization.[116,117]

4. Selectivity and reproducibility

The membrane sensor with an optimized shear protocol hence can outperform equilibrium surface assays in both sensitivity and selectivity.[111,118,119] We have quantified miR146a and miR550 (oral and pancreatic cancer biomarkers, respectively) in raw cell culture lysate and culture media with and without off-chip RNA extraction steps. We have also successfully detected longer RNAs, including discrimination between two different dengue virus (DENV) serotype RNAs, and between Brucella RNA and two-base mismatch control samples. Figure 4(a) shows the I-V shift upon detection of 2 pg/μl Brucella, while no shift is observed when DENV-2 mRNA is used as non- target, demonstrating our device selectivity. Figure 4(b) shows the I-V shift for DENV-2 at 50 pg/μl in a mixed sample with all four dengue serotypes. An I-V shift was observed only with DENV-2 RNA present in the mixture, confirming the sensor's ability to detect a specific target in a heterogeneous RNA population with similar sequences.

5. Limit of Detection (LOD)

Our biochip LOD depends on its ionic-membrane sensor area.[114,118,119] By reducing the sensing area from 0.25 mm^2 to 0.0625 mm^2, we improved the LOD by 3 orders of magnitude (to 10^4 copies per 100 μl), at the expense of some robustness. Samples with different ionic strengths and miRNA-550 concentrations from 1 pM to 1 μM were tested on 5 different chips (Fig. 4(c)). From these data, we estimated a universal Langmuir hybridization dissociation constant of $K_D \sim 500$ pM, which is about 3 orders of magnitude lower than literature values because of the preconcentration step (Fig. 4(d)).[119] These extensive studies clearly demonstrate the sensor is capable of rapidly quantifying miRNAs from 10^6 to 10^9 copies with minimum loss and high specificity. Its sensitivity exceeds conventional microarray assays by a factor of 10^2–10^3.

B. Bipolar-membrane technology for control of local pH

We have recently reported a bipolar-membrane technology that allows precise control of the pH in microfluidic devices. This module can provide a high pH that may be used for

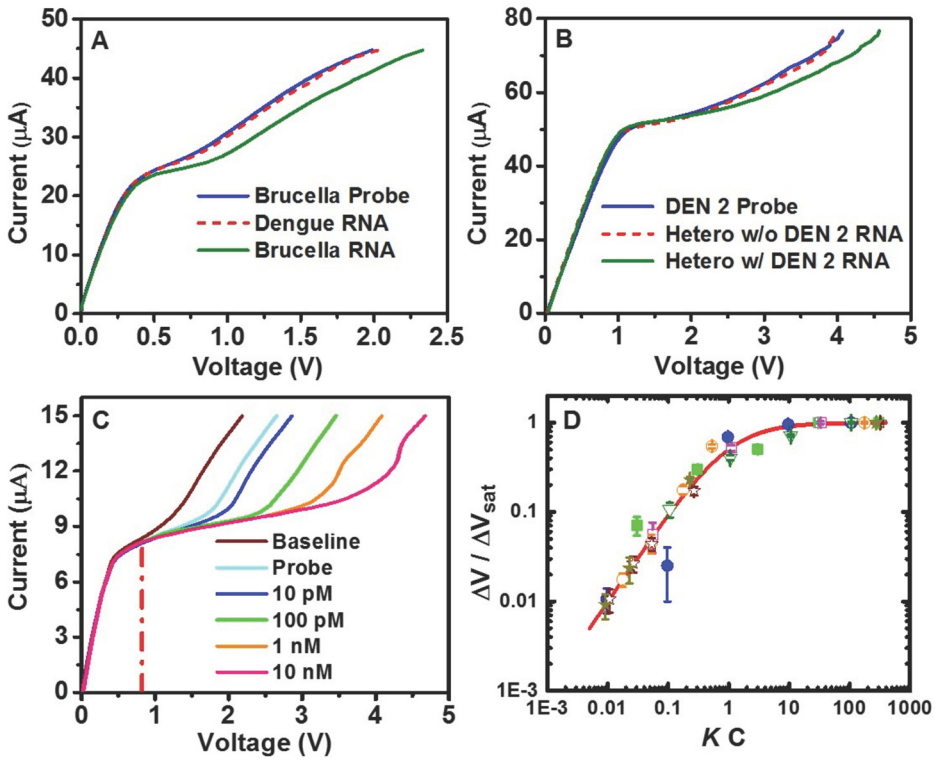

FIG. 4. RNA detection using a ionic-membrane sensor. (a) I-V characteristic or a 3.5 mm^2 ionic-membrane sensor, functionalized with a Brucella capture probe before (blue line) and after the addition of Brucella RNA at 2 $pg/\mu l$ (green line). Addition of a non-target RNA (Dengue virus) does not produce a shift in the I-V characteristics (red dotted line). (b) Detection of Dengue virus serotype 2 (DENV-2) RNA at 50 $pg/\mu l$ in a sample with mixed serotypes 1 to 4. (c) Voltage shifts for miR550 concentrations 10 pM to 1 nM (corresponding to 10^7–10^9 miR550 copies) spiked in conditioned cell culture media. (d) Calibration curve of the voltage shift vs. miR550 concentration, averaged over 7 different sensors, along a 3-decade dynamic range starting at 1 pM (10^6 copies). The Langmuir constant K ∼ 1/500pM indicates saturation at about 1 nM. Adapted with permission from Biomicrofluidics **60**, 92–100 (2014). Copyright 2014 AIP Publishing LLC;[118] and from Taller *et al.*, Lab Chip **15**, 1656–1666 (2015). Copyright 2015 Royal Society of Chemistry.[119]

dehybridization and elution of a target trapped in gels, bead packs, and membranes; and enhancement of the selectivity of the different hybridization assays described in this article. Briefly, pH actuation is based on a micro-scale bipolar membrane chip that can control the local pH in microfluidic chips without the introduction of external buffer (Fig. 5(a)).[120,121] These membranes, synthesized by UV photo-polymerization, exhibit distinct hysteretic *I-V* polarization and cyclic voltammetry signatures due to local field-induced water-breaking reactions. At the membrane junctions, a high-voltage reverse bias depletes ions and a large field

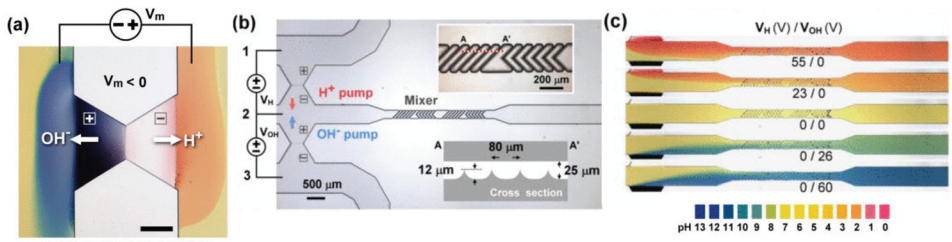

FIG. 5. Bipolar membrane technology. (a) Acidic and basic streams from water-splitting at bipolar-membrane proton and OH^- pumps. Color is from a pH-indicator dye. (b) Schematic representation of a pH actuation module with a proton pump, an OH^- pump, and a static mixer. Inset: expanded view of the mixer section. (c) Precise pH control by mixing proton and OH^- streams using external circuitry. Adapted with permission from Biomicrofluidics **5**, 046502 (2011). Copyright 2011 AIP Publishing LLC.[120]

($>10^6$ V/cm) develops. When the field exceeds the critical value of about 10 MV/cm, in accordance with the second Wien effect,[122] water dissociates irreversibly into H^+ and OH^-. These ions are then separated into their respective ion-selective membranes, creating two streams with very different pH (Fig. 5(b)). Acidic and basic streams from two bipolar membranes can be combined by a static mixer to achieve precise pH (Fig. 5(c)).

C. Extracellular vesicle lysing technology

Extracellular vesicles (EVs) are vesicles containing short nucleic acids (mRNA and miRNA) and proteins, perceived to be carriers of this cargo between diverse locations in the body, secreted by all types of cells in culture, and also found in abundance in body fluids.[123] EVs include exosomes (30–120 nm) and microvesicles (100–1000 nm). The nucleic acids and other molecular cargo in EVs hold promise as a source of biomarkers.[124] However, one of the factors that limits the discovery and application of EVs biomarkers is the burden of the extraction process. Ultracentrifugation is the most common method used for separation of EVs. It takes 4–5 hours, has a low yield (5%–25% recovery), and requires a capital cost around $50–100 k and a running cost of $3 k per year. Immunoaffinity techniques can be used for purification of a particular population of EVs with a specific surface marker in 2–4 h, but they are not better in terms of cost or complexity, nor can they isolate vesicles that do not have the specific capture marker. Commercial precipitation kits are easy to use and do not require any expensive equipment, but require a lengthy overnight incubation, their mode-of-action has not been disclosed, the purity of the acquired EVs has been reported to be inferior compared to other methods, and the chemicals from the precipitation kit may contaminate and affect the biological activity of the EVs. Finally, microfiltration and other size exclusion methods can suffer from clogging, shear stress-induced damage and analyte loss.[125] The process that follows typically takes 5–8 additional hours, and consists of exosome lysing and mRNA or miRNA detection by qRT-PCR or microarrays. As a result, the overall time for EV RNA analysis typically requires 8–12 h and multiple instruments, chemical kits and washes, which leads to considerable nucleic acid loss.

We recently developed a quantitative exosome miRNA biomarker assay using a microfluidic platform, which integrates separation of exosomes from a complex biological fluid by a size-exclusion filter; exosome lysis by surface acoustic wave (SAW); and sensitive and specific detection of target mRNA and miRNA using an ion-exchange membrane (IEM) sensor.[119] Lysis was achieved via surface acoustic waves (SAWs), which are Rayleigh waves generated on the surface of a piezoelectric crystal by alternating current applied through an interdigitated electrode transducer. When the SAW waves interact with a bulk liquid droplet or film, scattered sound waves produce an acoustic pressure in the liquid bulk while the electric component of the wave produces an electric Maxwell pressure at the solid liquid interface. In our experiments, the SAW-based exosome lysis rate achieved was 38%, which compares favorably to the typical 5%–25% recovery of EVs via centrifugation. These experiments were carried out using very small sample volumes ($\sim$100 μl). The detection sensitivity was very high ($\sim 10^{-6}$ copies of miRNA). All the operations were done within one chip, which further limits any loss of the target. From the raw sample to miRNA quantification, the analysis was performed in about 60 min, much faster than with current techniques. This platform may be scaled up for miRNA panels and large sample numbers required in biomarker discovery and disease screening/prognosis.

D. Polymer nanopores and nanopipettes

Nanopore sensing is based on the detection of electrical current produced by charged molecules transiting through nanopores (translocation), which can be used for counting individual biomolecules.[126] The single-molecule sensitivity and simplicity of nanopore sensors make them attractive for PCR-free, POC quantification of miRNAs with small copy number. Nanopore quantification can outperform the traditional surface assays in sensitivity because it does not rely on reversible hybridization. The most common nanopore types are short and small (<1 nm) "soft" protein pores,[127–129] conic solid-state pores,[130,131] and a hybrid of the two as in the Oxford Nanopore technology with a gating motor protein at the end of a solid-state nanopore.

Protein nanopores can achieve single miRNA molecule detection and single mismatch discrimination using probes with ion-current tags produce distinct signatures during transit through protein nanopores.[127–129] Still, protein nanopore technologies suffer from several shortcomings that must still be resolved. These nanopores are very unstable and are often clogged by long RNAs with secondary structures and bound proteins. Extensive sample preparation and purification is required before a few miRNA molecules can be quantified.[132] Their throughput is prohibitively low for POC applications. (It would take more than one hour to interrogate 10^3 molecules.) Target molecule loss due to non-specific adsorption onto micro/nanofluidic devices is also a problem. Most studies report that only 10^5 or fewer molecules can be driven through a single nanopore per hour, due to long transport times to the pore and, in the case of protein pores, long translocation time. Since a cell typically contains 10^2–10^4 miRNA molecules and 10^{10} other nucleic acids and proteins, it would take from 1 to 10^5 h to interrogate all these molecules with a single pore, assuming large genomic DNA and rRNA-protein complexes do not clog the pore. These issues have limited protein nanopore sensors to applications where the target in the starting sample is isolated from the other molecules by extensive pretreatment and/or amplified using PCR.

Larger conic solid-state nanopores are more stable than protein pores, and allow transit of bigger nucleic acids or RNA-protein complexes, but have translocation times that are too short (μs) to differentiate or even register the subtle ion current signals of short mRNA (<100 bases) and miRNAs (18–22 bases).[126] Radioactive and ion current tags used to detect ssDNA and miRNA protein pore translocation do not produce distinct signatures during fast transit through solid-state pores. Gating oligonucleotides functionalized on solid-state nanopores can delay the translocation of long ssDNA.[126] However, for short miRNAs, translocation and radial diffusion times are comparable and approach the surface-probe binding kinetic time. Moreover, hybridization can block further molecular transit through the pore, thus compromising the throughput. Hybridization of miRNA or short ssDNA to specific probes functionalized on solid-state nanopore tips during field-driven translocation has yet to be reported.[133]

We envision that by integrating different technologies described in this article, current nanopore technology limitations may be overcome. The probe-based capture unit described in Section IV A 3 can capture fewer than 10^6 copies of the target nucleic acid using smaller membranes (10–100 μm) functionalized with oligo-probes. Although this copy number cannot be robustly quantified by ionic current measurements because the current approaches the thermal shot noise for such micron-sized membranes, the probe-functionalized membrane can still serve as an intermediate target extraction unit. Hybridized target molecules may be released by either thermal melting, or high pH flushing using the bipolar membrane module described in Section IV B. A downstream nanopore module would then quantify the released targets. With the multi-stage purification steps offered by the integrated membrane platform described in Section IV A, the analyte would be within the narrow dynamic range of the nanopore technology and hence precise quantification could be carried out.

There are several low-cost nanopore fabrication technologies for making single and multiple solid-state nanopore membranes (see, for example, laser-assisted pulling and ion-track fabrication technologies that we have employed[134–138]). Among these, track etching of polyethylene terephthalate (PET) polymer membranes and chemical etching can produce solid-state conic nanopores with very small tip diameters ranging from 5 to 10 nm. These technologies can be also used to fabricate multi-nanopore PET membranes with 10^4–10^6 pores per square millimeter for high throughput. Laser assisted pulling can be used to fabricate conical nanocapillaries several cm long with a tip diameter ~100 nm. Although these technologies are not quite ready yet for mass production, they could be achieved with some industrial development.

E. Field-controlled nanoparticle assemblies for specific miRNA capture

Another alternative for low-copy miRNA quantification is optical sensing. Optical sensing has high sensitivity but requires extensive pretreatment, which can be achieved with the pretreatment modules of Section IV A. Optical sensors and in particular, plasmonic sensors, often

require expensive nanofabrication, and transport and concentration of analytes from the bulk onto the nanostructures. A low-cost alternative for transport, concentration and specific capture of miRNAS is packing probe-functionalized nanoparticles (NPs) within nanocapillaries and conic nanopores. These nanostructures can delay hybridized target molecules translocation times, under high electrophoretic and electro-osmotic shear to prevent non-target hybridization.

We have developed protocols for assembly of cells,[139–141] micro/nanocolloids,[142–145] vesicles,[140] and viruses[146] by enhanced electric forces at sharp geometries.[147–152] For example, we can pack 25 nm to 100 nm oligo-functionalized Au, silica and polystyrene NPs into ion-track etched polyethylene terephthalate (PET) polymer conic nanopores,[134,135] and into conic silica nanocapillaries pulled by laser assisted drawing.[130,136,137] We have studied the NP assembly mechanism with two-dimensional nano-wedge models fabricated by focused ion beam milling.[153] In a conic nanopore, NPs larger than the conic tip diameter ($\sim$100 nm) can be assembled by electrophoresis either on its tip or through its base. NPs packed on the tip can be disassembled with a reverse bias. In contrast, intra-pore NP assembly is irreversible.

Assembling NPs smaller than the tip size is more challenging. We have found two field-induced phenomena that can trigger small NP assembly within these nanoconstrictions: intrapore ion enrichment/depletion and trapping of co-ion NPs by isotachophoresis. Upon the application of a voltage across an ion-track nanopore, since its dimensions are comparable or smaller than the Debye layer, large longitudinal ionic strength and conductivity gradients are induced near the tip.[134] Due to the pore's long aspect ratio, cross-section electro-neutrality exists. The mobile charge density scales as the inverse of the local nanopore radius R^{-1} to balance the immobile surface charge. In our conic pores, most of the mobile ions are counter-ions, and hence the ionic strength also scales in the same manner. A more rigorous theory can be found in our theoretical work.[134,135,154] Since the focusing field in this conical geometry scales as R^{-2}, ion flux cannot be continuous and ion accumulation/depletion ensures to maintain local neutrality. With an applied positive voltage, the large longitudinal ionic strength and conductivity gradients increase the intra-pore ionic strength by a factor as high as 10 to beyond 1 M. In fact, such intra-pore enrichment and its depletion counterpart at negative bias are responsible for the ion current rectification observed in conic pores and wedge-shaped channels at low voltage.[134,153] At high voltages, external depletion and enrichment[110,113,155–159] causes an inversion of the rectification factor.[134] Internal enrichment conditions can induce intrapore NP assembly. Equilibration with the bulk stipulates that the enriched ionic strength within the pore exhibits a maximum at a distance from the tip that is roughly equal to the tip diameter. The longitudinal electric field also reaches a minimum at this maximum enrichment location. Co-ion NPs can hence be enriched with other ions from the base, or be packed there by isotachophoresis due to a nearly discontinuous drop in their flux at that location.[160] If the local ionic strength at the packing location exceeds the critical flocculation value for charged Au NPs (roughly 0.5 M,[143] or lower with field), the packed NPs irreversibly assemble into dense aggregates. Our SEM and fluorescent images of the NP assemblies within the nanocapillary and nanopore reveal small assemblies roughly at the location of the ionic strength maximum.

We have demonstrated specific capture of miR146a while permitting rapid transit of non-targets including a similar miR146b, by tuning the spacing of 25 nm NP assemblies packed into 100 nm conic nanocapillaries using an electric field. Validation was done with hairpin probes for miR146a with fluorescent reporters and quenchers enhanced by NP plasmonic hotspots.[136,161] Gold NPs were functionalized with a thiolated fam-labeled hairpin oligo-probe (HOP) (Fig. 6(a)). In this example, an unpaired 22-base loop is complementary to the miRNA target. Upon hybridization, the probe becomes rigid and pushes the fluorescent reporter away from the quenching metal NP so that it produces a fluorescent signal. However, quenching still exists; the quantum yield of the fluorescent reporter is never as high as a free reporter in the bulk.[162–164] For this reason, planar and single-NP Surface Enhanced Fluorescence (SEF) cannot exceed 10-fold enhancement.[161–166] This limitation can be overcome by plasmonic hotspots between NPs packed with 10 nm gaps,[167] from which enhancement as high as 10^4 for a single molecule has been reported.[164] We used an electric field to control spacing of small NPs assembled within a conic nanocapillary and produce plasmonic hotspots with maximum SEF

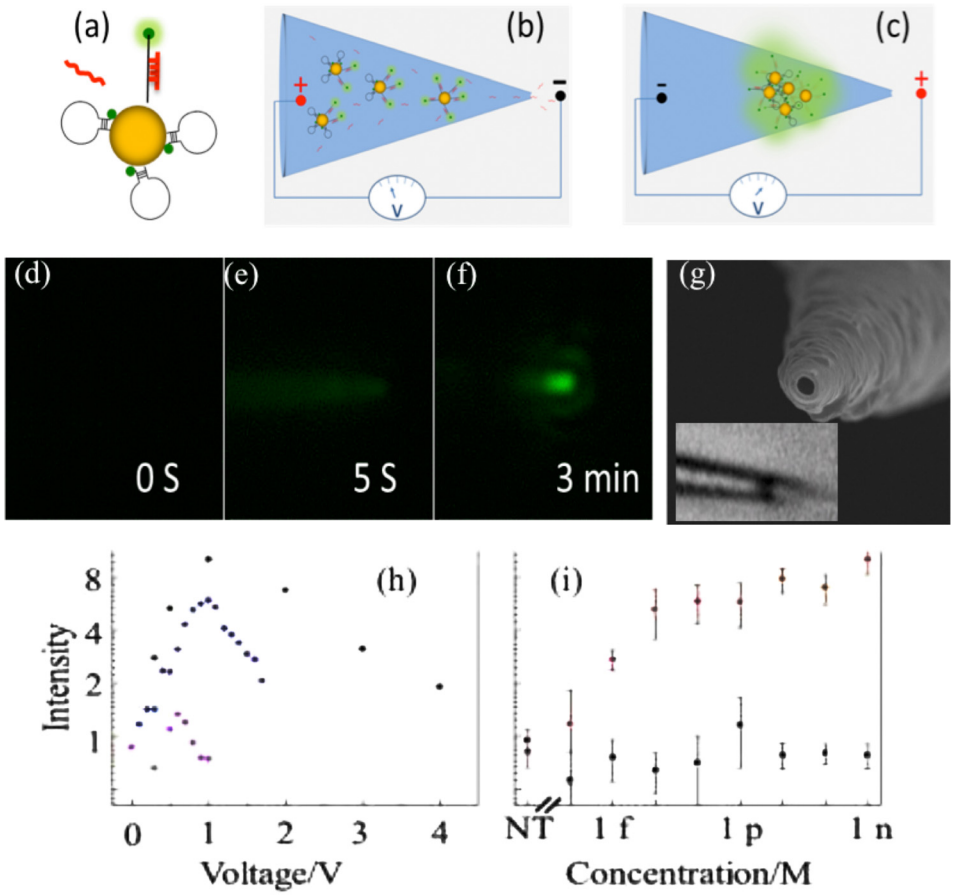

FIG. 6. Hairpin Oligo Probe (HOP)-functionalized AuNPs nanopore-based detection. (a) Upon target hybridization the fluorophore (green dot) is displaced beyond AuNP quenching distance. (b) Target miRNAs and HOP-AuNPs are driven into a conic nanocapillary by a negative voltage. (c) Voltage is reversed to aggregate AuNPs, promote hybridization, and plasmonically enhance fluorescence. (d)–(f) Microscopy sequence of HOP-AuNP packing and target miRNA hybridization in a silica conic nanocapillary; a negative voltage is applied at t = 0s and reversed at t = 10s; the plasmonically enhanced fluorescent signal is evident at t = 3 min. (g) A 100 nm nanocapillary tip SEM. Inset: light microscope image of a micron-sized 25 nm-NP aggregate inside the silica nanocapillary. The inner nanocapillary diameter is about 150 nm at the aggregate location; its distance from the tip (∼1 μm) corresponds to the ionic strength maximum in Fig. 9(a). (h) miRNA hybridization across a AuNP assembly in a conic glass nanocapillary: fluorescence intensity vs. voltage after target and non-target hybridization. (i) Fluorescent intensity for the target and for a 3-mismatch in the 23-nucleotide miRNA at different concentrations indicating little hybridization of the latter. Adapted with permission from Biomicrofluidics **7**, 061102 (2013). Copyright 2013 AIP Publishing LLC.[136]

for HOP-NPs. In order to pack the target and nanoparticles in the nanopores, we used a two-step field program. First, field-enhanced adsorption was used to promote hybridization onto the probe functionalized NPs; and then a reverse (and ramped) bias was used to pack the NPs (Figs. 6(b) and 6(c)). The onset of SEF fluorescence signal (Figs. 6(d)–6(f)) permits us to monitor the NP assembly dynamics, location, size, and spacing.[136] Computer simulations show that the NP assembly location coincides with the counter-ion concentration maximum under enrichment conditions (Fig. 6(g)). The LOD for miR146a was about 1000 copies. A two-base mismatch miR146b produces a much weaker fluorescence, suggesting that the probability of non-targets being captured through the assembly is insignificant (Fig. 6(i)). Non-targets with larger number of mismatches were not detectable at all.

This LOD is far below its dissociation constant, confirming that the field-assisted hybridization first step is irreversible. While irreversible adsorption may promote non-specific binding, the ramped electric force and electro-osmotic shear remove the non-targets during the second packing step. Sequential irreversible adsorption and desorption hence may outperform

equilibrium adsorption/desorption in both sensitivity and selectivity. We have begun to scrutinize this irreversible hybridization mechanism during fast translocation across NP assemblies. We have found that the fluorescent intensity (hybridization efficiency) exhibits a maximum with respect to the driving voltage for miRNA translocation (Fig. 6(h)). This suggests that beyond a critical voltage, the target translocation speed may be too high to allow hybridization. Selective capture of 1000 miRNA targets in the conic nanocapillaries has therefore been achieved with significant throughput with this optimized NP assembly.

With tip diameters smaller than 100 nm, the field at the tip exceeds kV/cm, and the translocation speeds mm/s. We estimate that the shear rate within a NP assembly in one of these small nanopores can be as high as $10^4\,s^{-1}$. This rate exceeds the critical shear rate required to dehybridize dsDNAs (about $300\,s^{-1}$.)[113,115] Similar order of magnitude electrophoretic[116,117,168] and mechanical AFM[169] dehybridization forces have been reported. Hence, it is necessary to lengthen the translocation time of miRNA beyond 10 ms for hybridization in a small conical nanopore. This may be done by assembling NPs of different sizes and materials inside the nanopores. As in our earlier studies with nanoslots, dielectric NP packing may be monitored by DC and AC impedance characterization.[170–172] However, we believe a fundamentally different approach must be used to capture miRNAs using NP assemblies in conic nanopores with tips smaller than 50 nm.

F. Conical solid-state nanopores with alumina films as miRNA counters

We have developed a technique for Atomic Layer Deposition (ALD) of dielectric (alumina) atomic layers inside etched ion-track PET nanopores.[134,135,173] ALD can be used to tune nanopore tip diameters from 5 nm to 100 nm, and to prolong translocation times by reversible adsorption due high-permittivity alumina layer van der Waals (vdW) forces at the smaller tips (Fig. 7). We have found that short 22-b ssDNA (a miRNA mimic) has much higher affinity for the alumina layer than their dsDNA counterpart. When driven from the tip side of an alumina-coated nanopore, the translocation time of a 22-b ssDNA molecule is between 10 ms and 1 s, one to three orders of magnitude longer than the millisecond translocation time of a dsDNA molecule of the same contour length. This is the longest translocation time reported. In fact, 22-bases is the shortest ssDNA that has been reported to produce a resistive pulse signal in solid-state pores. We suspect the exposed rings of the ssDNA with delocalized electrons produce a larger Hamaker constant and vdW attraction to the tip wall. Figure 8(a) shows that the translocation events are initially dominated by the more rigid dsDNA (1 ms pulses), while the ssDNAs only begin their translocation after 10 min. This suggests that ssDNA first adsorbs onto the alumina-covered substrate before migrating along the inner nanopore surface to the nanopore. Indeed, super-resolution stimulated emission depletion (STED) imaging of the alumina-covered substrate (Fig. 8(b)) after 30 min shows a ssDNA-depleted ring around the conic tip. In order to delay the translocation time of miRNAs, tip-side functionalization[174] for attaching probes onto the alumina nanopores may be the best alternative to achieve specific capture. The nanopore ohmic heating technology described in Sec. IV G may be used to produce an elevated temperature at the tip and achieve highly localized probe functionalization.

G. Nanopore ohmic thermal programming

A combination of nanocapillaries and/or multi-pore membranes can be used for target separation, followed by single nano-pore modules for precise target counting. Nanopore ohmic heating may be used to achieve highly selective, quantitative detection of targets with low copy numbers. Thermally enhanced selectivity occurs when probes are functionalized onto the nanopore alumina film to selectively capture specific targets. Since non-target complexes with the probes have a lower melting temperature than those involving targets, temperature ramping and other programming protocols can potentially remove the non-targets during or after the complex formation process. Moreover, after non-targets are removed, captured non-targets may be then released by an even larger thermal ramp, and directed to a single nanopore miRNA counter (Fig. 8). Control of the nanopore temperature may also enable preferential functionalization of

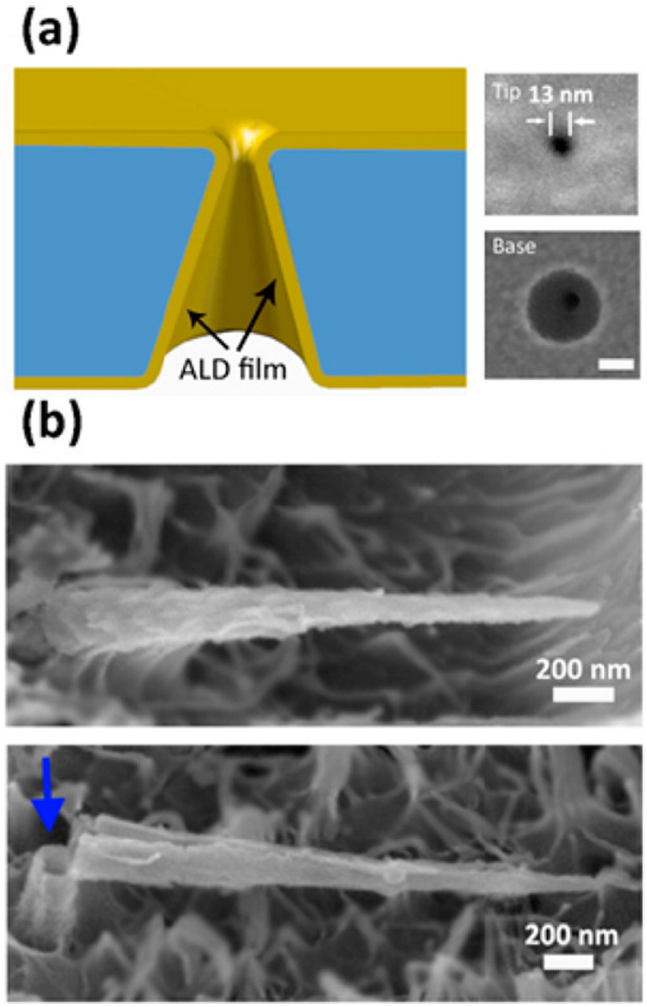

FIG. 7. (a) Schematic illustration of uniform ALD coating on a single conical nanochannel (not to scale). Insets show SEM images of the tip side (top) and the base side (bottom) of an ALD Al2O3-coated polymeric conical nanochannel. Scale bar = 100 nm. (b) SEM images of conical Al2O3replicas obtained by coating the conical nanochannels by 150 cycles of ALD Al2O3 and then treating with RIE to partially remove the PET polymer matrix. A broken part of the Al2O3 replica (blue arrow) revealed that the ALD coating was only on the pore wall, indicating excellent step coverage inside the nanochannels. Adapted with permission from Wang *et al.*, Anal. Chem. **87**, 16 (2015). Copyright 2015 American Chemical Society.[183]

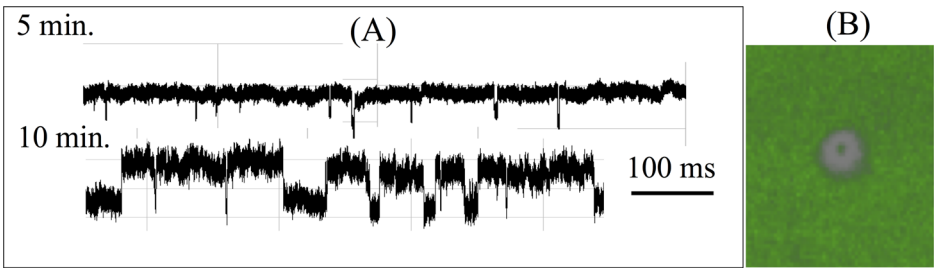

FIG. 8. (a) Translocation resistive pulse signals of a 50-50 mixture of 22 b ssDNA and dsDNA after 5 min and 10 min. Average ssDNA translocation time is about 100 ms, compared to the average dsDNA translocation time of 1 ms. The distinctly different translocation times allow easy identification of the two events. The longer ssDNA translocation events initiate only after 10 min. (b) STED super-resolution microcopy image at 30 min shows that this delay of ssDNA translocation is due to an adsorption step onto the membrane surface before migration into the tip (see 100 nm depletion ring in the image).

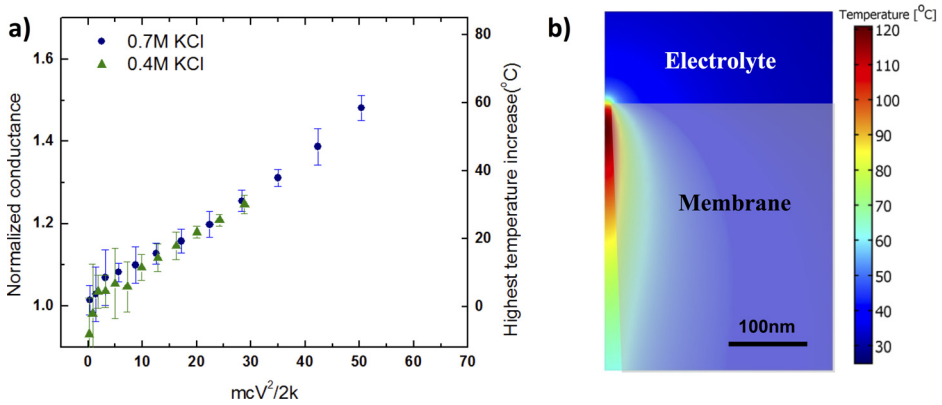

FIG. 9. (a) Measured average conductance normalized by the zero voltage value as a function of the voltage (V) and ionic strength in molarity (M) for a single pore polymer membrane. Right vertical axis: temperature increase at corresponding normalized conductance predicted by simulation. The error bar is the standard deviation of three times of measurement. b) Numerical simulation of the nanopore temperature shows a hotspot about 100 nm in linear dimension and with a maximum temperature exceeding 85 °C.

probes onto the nanopore tips, minimizing the target loss that would result from target being captured by probes on other areas of the nanopores. Due to miRNA short length, slight sequence variations can produce differences in melting temperatures of hybridized target-probe complexes as large as 20 °C. While this melting temperature variation is detrimental to miRNA qRT-PCR normalization and efficiency, it can be exploited to enhance selective hybridization in the nanopore technologies. This thermal programming should ideally be confined to a very small region—at the tips of individual nanopores. A micro-heater that heats up the entire chip would not allow independent modular operation. Instead, with each nanopore module having its independent thermal programming, the integrated platform may achieve profiling of many targets with small copy numbers.

Conic PET nanopores offer a unique localized heating phenomenon for this purpose. Nagashima *et al*. recently discovered uncontrolled bubble cavitation in a single cylindrical nanopore due to intense Ohmic heating.[175] Current blockage due to bubble cavitation at the tip is observed beyond 120 °C (Fig. 9(a)) due to a significant nano-capillary effect.[175] Nevertheless, a temperature range between 30 and 100 °C may be achieved. By increasing the voltage beyond the range typically used to study molecular translocation, we can establish a stable elevated temperature at the nanoscale conic tip to selectively capture and release a small number of miRNAs.

In conical geometries, field-focusing effects can be used to develop a steady nanoscale thermal hotspot. We took advantage of these effects at cones and wedges in the development of AC sprays and nano-aerosolization technologies.[84–89] Similarly, these effects may be used for thermal programming in PET conical nanopores. The local Joule heating density increases rapidly towards the tip due to field focusing, $\sigma E^2 = \sigma E_0^2 (R/r)^4$, where σ is the local conductivity, E_0 is the nominal field proportional to the applied voltage V, and R is the radial position of the base in the spherical coordinate r that traverses the cone axis. Inserting this localized heat source into the radially symmetric conduction equation, one obtains a temperature increase from the ambient that increases as $\frac{\sigma E_0^2}{2k}\left(R^4/r^2\right)$ towards the tip at $r = r_{tip}$. The hot spot temperature at the position of the tip $r = r_{tip}$ then predicts a hot spot temperature rise and this hotspot is localized within a region at the tip whose ($\sim$100 nm) spatial dimension scales as $(\sigma/kT_\infty)^{1/2} E_0 R^2 \sim \sqrt{\sigma} V$. If we now consider, to the next order, the linear increase in the local conductivity with respect to temperature due to viscosity decrease, the ion current conductance of a given single or multiple cone membrane is found to be only a function of MV^2, where M is the bulk ionic strength (through σ). Without Ohmic heating at the tip, the conductance would be independent of the voltage V. As shown in Fig. 9(a), this universal scaling with respect to the voltage and ionic strength is indeed experimentally observed in single-pore membrane conductance measurements in the high ionic strength limit, when surface charge-induced

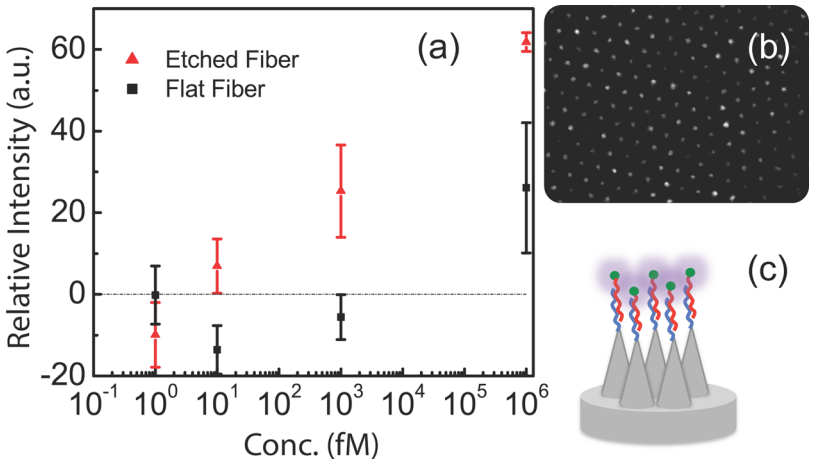

FIG. 10. Nanocone array. (a) Relative fluorescence intensity subtracted by blank sample was plotted vs. concentration in semi-log scale. The intensity value is relative values from CCD camera. (b) Fluorescence image from hybridized miRNAs labeled with fluorescence dyes. c) Schematic of etched cones, functionalized with oligo-probes at the end of an imaging fiber bundle. Adapted with permission from Biomicrofluidics **8**, 021101 (2014). Copyright 2014 AIP Publishing LLC.[176]

intrapore enrichment/depletion and rectification effects are offset by taking the average of conductance of positive and negative biases.[134] We have also scaled away dependence on the cone geometry and number by normalizing with respect to the conductance at the zero-voltage limit. The scaling theory and data are consistent with COMSOL simulation (Fig. 9(b)) which shows a steady hotspot with a dimension of about $l \sim 100\,\text{nm}$ at 24 V.

H. Nanocone array technology

Recently, we reported a hybridization sensor based on a nanocone array fabricated by wet-etching an imaging fiber bundle section (Fig. 10). In this proof-of-concept work, we detected a single miRNA target. However, since each of the tens of thousands fibers in the bundle can be individually addressed, this platform has potential for multiplex profiling. It uses point (10 nm–1 μm) illumination of preferentially adsorbed, fluorescently labeled targets by singular scattering at wedged cones. Fluorescent spots with diffraction-limited submicron dimensions have areas 10^4 times smaller than conventional microarrays. This reduction in area brings a comparable reduction in detection limit to 100 molecules per tip for a 10 fM bulk concentration (four orders of magnitude better than any existing technology) and an amplification of dynamic range to 6 decades, from femtomolar to nanomolar concentrations (Fig. 10(a)).[176,177]

Commercially available fluorescent micro-arrays based on target labeling, northern blot, or enzyme-linked immunosorbent assay (ELISA) are limited to a detection limit of $1–10 \times 10^6$ molecules per fluorescent spot, thus requiring cell culture or PCR amplification. This low sensitivity is often due to broad illumination, which creates auto-fluorescence noise. Even with point illumination and pin-hole filtering of non-focal plane noise in a confocal setup, the large and non-uniform fluorescent spots create scattering noise over each 20–100 μm element, which degrades the detection limit. Smaller spots might, in theory, be introduced by nano-sprays and nano-imprinting. However, directing the targets to such small areas then becomes problematic.

We employed a well-defined multi-wedged silica nano-cone array fabricated by wet-etching an imaging fiber 2 mm thick slice. The wedges are introduced by non-uniform stress formed during the imaging fiber bundle assembly process. Maximum scattering occurs at the tip where three to four wedges converge. We used the reflection mode to fully exploit this singular scattering to excite fluorescent reporters at the tip and transmit the resulting signal (Fig. 10(c)). In our sensor, field focusing at the cone tip by the dielectric media (the silica fiber) is used to produce a localized and singularly large scattering intensity at the tip (Fig. 10(b)). Numerical simulation has revealed that field focusing by this singular scattering can effect a five-order intensity enhancement that is frequency independent.[178,179] Intense scattering at the

tip acts as a local light source that does not suffer from conduction loss. Unlike plasmonic metal nanostructures, the dielectric tip does not quench the fluorescent reporters excited by the light source. In fact, it can help scatter the fluorescent signal, with Rayleigh scattering intensity scaling with respect to the wavelength. We hence utilized this phenomenon for diffraction-limit fluorescent sensing/imaging. The local light source due to tip scattering minimizes background auto-fluorescence and scattering noise. In addition, we have found that the target molecules preferentially diffuse towards the dielectric vertices.

These dielectric nano-tips may provide the smallest fluorescent spot that can preferentially capture target molecules and whose fluorescent image is limited in size only by the diffraction limit, without a confocal configuration. Since these nanostructures can be fabricated using low-cost methods, they may be amenable for portable multiplexed detection.

I. Nanoparticle aggregation for short nucleic acid quantification by depletion isotachophoresis

We have recently developed an electrophoretic technology for rapid, selective, colorimetric detection of nucleic acids based on nanoparticle aggregation and depletion isotachophoresis.[180] It significantly enhances the sensitivity of nanoparticle assays and the selectivity of electrophoretic assays for nucleic acids of the same length. This microfluidic chip uses a combination of Au nanoparticles (AuNPs), ion-selective membranes, and gel electrophoresis to detect and identify single-stranded DNA targets with roughly the same length as ctDNA. The chip is composed of a straight channel a couple centimeters long with an ion-selective membrane fixed above the channel downstream of the sample inlet. A mixture of probe-functionalized AuNPs and target DNA is driven by electrophoresis through the gel, until AuNPs are packed against the ion-selective membrane. The close packing enhances the hybridization rate between probes and target. Upon hybridization, nanoparticles become linked into dimers. Upon reversing the electric field, the high shear in the gel selectively breaks up dimers formed by the non-targets. Due to the ion-selective membrane, the reversed field also forms a region depleted of ions that extends along the channel. The disparity in ionic strength between the depletion region and the concentrated ion front at the fore of the depletion zone allows separating the dimers from the monomers as follows. While the high electric field in the depletion zone selectively aggregates the dimer particles until they become too large to pass through the pores of the gel, the field shears away the monomers, so the two bands can be clearly distinguished. For a 69-base target, the assay can detect down to 10 pM from a 2 μl sample volume in less than twenty minutes. It is highly selective against non-targets, which yield no appreciable signal. Furthermore, in heterogeneous mixtures where non-targets outnumber targets by a factor of 10 000–1, the targets signal intensities are comparable to signals from pure target samples. The selective nature of the chip is due to the high electric field facilitated by the depletion region. The force of the electric field disrupts nonspecific interactions thereby ensuring only fully hybridized pairs will be detected.

The strength of this sensing strategy resides in its ability to discriminate between target and non-target sequences that differ by only a few base pairs and have similar dissociation constants. In this biochip, continually ramping the strength of the electric field disrupts the increasingly strong non-target linkages while leaving the target linkages unperturbed. The electric shear force overcomes the weaker non-target interactions and therefore ensures that only target-linked particles aggregate. This assay may be amenable to multi-target sampling through the use of nanoparticles with different plasmonic frequencies or different fluorescent wavelengths.

V. CONCLUSIONS

Due to the diverse characteristics of biological matrices (e.g., serum, urine, saliva, etc.) and targets (mRNA, miRNA, and ctDNA), and the large dynamic range of the possible nucleic acid target concentrations, different pretreatment units and detection technologies will need to be integrated in each case. We hence envision a profiling platform with a modular design, where different detachable pretreatment, detection, and optical sensing modules can be assembled.

Such a multi-modular platform is ideally suited for a 3D chip architecture that can be realized by 3D printing prototyping.[181] Instrumentation should ideally be also reconfigurable so that it can easily accommodate the integrated modular platform.[134,135,173]

Future precision medicine will heavily depend on the ability to perform frequent liquid biopsies, and in general, on profiling various nucleic acids in serum and other physiological samples for screening, diagnostic, and prognostic applications in cancer and other diseases. However, broad availability of this future molecular medical approach requires new nucleic acid diagnostic technologies quite distinct from current ones. Our group has been working on several microfluidic and nanofluidic technologies in anticipation of such a transformation in health care. From our viewpoint, integration of these technologies in a modular design can offer a low-cost, robust and yet sensitive/selective platform for a variety of precision medicine applications. This perspective summarizes our strategy and we hope that it can also catalyze other approaches in this very promising direction for the microfluidics community.

ACKNOWLEDGMENTS

Our group has been supported by the Walther Cancer Fund 0120, USDA 2012-67005-19589, NSF-CBET 1065652, the Far Eastern Foundation, and NIH 1R21AI105361-01A1.

[1]P. A. Sharp, "The centrality of RNA," Cell **136**(4), 577–580 (2009).
[2]F. Ozsolak and P. M. Milos, "RNA sequencing: advances, challenges and opportunities," Nat. Rev. Genet. **12**(2), 87–98 (2011).
[3]S. A. Mortimer, M. A. Kidwell, and J. A. Doudna, "Insights into RNA structure and function from genome-wide studies," Nat. Rev. Genet. **15**(7), 469–479 (2014).
[4]M. Schmitt *et al.*, "Diagnosing cervical cancer and high-grade precursors by HPV16 transcription patterns," Cancer Res. **70**(1), 249–256 (2010).
[5]H. Schwarzenbach, D. S. B. Hoon, and K. Pantel, "Cell-free nucleic acids as biomarkers in cancer patients," Nat. Rev. Cancer **11**(6), 426–437 (2011).
[6]I. Lee *et al.*, "Discriminating single-base difference miRNA expressions using microarray probe design guru (ProDeG)," Nucleic Acids Res. **36**(5), e27 (2008).
[7]A. Git *et al.*, "Systematic comparison of microarray profiling, real-time PCR, and next-generation sequencing technologies for measuring differential microRNA expression," RNA **16**(5), 991–1006 (2010).
[8]Y. Zhao and A. R. Brasier, "Methods for biomarker verification and assay development," Curr. Proteomics **8**(2), 138–152 (2011).
[9]M. J. Duffy *et al.*, "Validation of new cancer biomarkers: A position statement from the European group on tumor markers," Clin. Chem. **61**(6), 809–820 (2015).
[10]F. Montani *et al.*, "miR-Test: A blood test for lung cancer early detection," J. Natl. Cancer Inst. **107**(6), djv063 (2015).
[11]N. Goossens *et al.*, "Cancer biomarker discovery and validation," Transl. Cancer Res. **4**(3), 256–269 (2015).
[12]L. Wu and X. Qu, "Cancer biomarker detection: recent achievements and challenges," Chem. Soc. Rev. **44**(10), 2963–2997 (2015).
[13]F. Leung, E. P. Diamandis, and V. Kulasingam, "Ovarian cancer biomarkers: Current state and future implications from high-throughput technologies," Adv. Clin. Chem. **66**, 25–77 (2014).
[14]L. Xing *et al.*, "Sputum microRNA biomarkers for identifying lung cancer in indeterminate solitary pulmonary nodules," Clin. Cancer Res. **21**(2), 484–489 (2015).
[15]P. Craw and W. Balachandran, "Isothermal nucleic acid amplification technologies for point-of-care diagnostics: A critical review," Lab Chip **12**(14), 2469–2486 (2012).
[16]M. J. Murray *et al.*, "Solid tumors of childhood display specific serum microRNA profiles," Cancer Epidemiol. Biomarkers Prev. **24**(2), 350–360 (2015).
[17]M. de Planell-Saguer and M. C. Rodicio, "Detection methods for microRNAs in clinic practice," Clin. Biochem. **46**(10–11), 869–878 (2013).
[18]C. Bettegowda *et al.*, "Detection of circulating tumor DNA in early- and late-stage human malignancies," Sci. Transl. Med. **6**(224), 224ra24 (2014).
[19]P. S. Mitchell *et al.*, "Circulating microRNAs as stable blood-based markers for cancer detection," Proc.e Natl. Acad. Sci. **105**(30), 10513–10518 (2008).
[20]E. Fernandez de Avila *et al.*, "Determinants of the detection limit and specificity of surface-based biosensors," Anal. Chem. **85**(14), 6593–6597 (2013).
[21]C. C. Pritchard, H. H. Cheng, and M. Tewari, "MicroRNA profiling: Approaches and considerations," Nat. Rev. Genet. **13**(5), 358–369 (2012).
[22]M. Baker, "MicroRNA profiling: Separating signal from noise," Nat. Methods **7**(9), 687–692 (2010).
[23]See https://www.accessdata.fda.gov/scripts/opdlisting/oopd/ for the complete list of companies that have applied for approval of RNA-targeting drugs. These include Lorus Therapeutics, Inc., Alnylam Pharmaceuticals, Senesco Technologies, Inc., Isis Pharmaceuticals, Inc., Quark Pharmaceuticals, Inc., TransDerm, Inc., ProQR Therapeutics B.V., Silenseed, Ltd., Rexahn Corporation, Arrowhead Research Corporation, and Shire.
[24]G. McClorey and M. J. Wood, "An overview of the clinical application of antisense oligonucleotides for RNA-targeting therapies," Curr. Opin. Pharmacol. **24**, 52–58 (2015).

[25]See http://www.fda.gov/medicaldevices/productsandmedicalprocedures/invitrodiagnostics/ucm330711.htm for a list of U.S. Food and Drug Administration approved Nucleic Acid Based Tests.
[26]J. Vermehren *et al.*, "Differences between two real-time PCR-based hepatitis C virus (HCV) assays (RealTime HCV and Cobas AmpliPrep/Cobas TaqMan) and one signal amplification assay (Versant HCV RNA 3.0) for RNA detection and quantification," J. Clin. Microbiol. **46**(12), 3880–3891 (2008).
[27]N. Rosas-Murrieta *et al.*, "Molecular diagnostics as an indispensable tool for the diagnosis of infectious diseases of viral origin and global impact," in *Trends in Infectious Diseases*, edited by Shailendra Saxena (InTech, 2014), Chap. 5, pp. 89.
[28]N. Grüner *et al.*, "Performance characteristics of the VERSANT hepatitis C virus RNA 1.0 (kPCR) assay," Int. J. Med. Microbiol. **305**(7), 627–635 (2015).
[29]E. D. Deeks, "COBAS® AmpliPrep/COBAS® Taqman® HCV Quantitative Test, Version 2.0: An *in vitro* test for Hepatitis C virus RNA quantification," Mol. Diagn. Ther. **19**(1), 1–7 (2015).
[30]J. Vargo *et al.*, "Clinical specificity and sensitivity of a blood screening assay for detection of HIV-1 and HCV RNA," Transfusion **42**(7), 876–885 (2002).
[31]E. Munson *et al.*, "Comparison of commercial hybridization and automated transcription-mediated amplification modalities for detection of high-risk human papillomavirus nucleic acid," J. Clin. Microbiol. **52**(1), 331–334 (2014).
[32]M. Rebolj *et al.*, "Prevalence of human papillomavirus infection in unselected SurePath samples using the APTIMA HPV mRNA assay," J. Mol. Diagn. **15**(5), 670–677 (2013).
[33]J. Munkhdelger *et al.*, "Comparison of the performance of the NucliSENS EasyQ HPV E6/E7 mRNA assay and HPV DNA chip for testing squamous cell lesions of the uterine cervix," Diagn. Microbiol. Infect. Dis. **79**(4), 422–427 (2014).
[34]S. E. Capaul and M. Gorgievski-Hrisoho, "Detection of enterovirus RNA in cerebrospinal fluid (CSF) using nuclisens easyq enterovirus assay," J. Clin. Virol. **32**(3), 236–240 (2005).
[35]G. Cloherty *et al.*, "HCV RNA assay sensitivity impacts the management of patients treated with direct-acting antivirals," Antivir. Ther. (Lond.) **20**, 177–183 (2015).
[36]M. Fernandez-Mercado *et al.*, "The circulating transcriptome as a source of non-invasive cancer biomarkers: concepts and controversies of non-coding and coding RNA in body fluids," J. Cell. Mol. Med. **19**(10), 2307–2323 (2015).
[37]P. Economopoulou *et al.*, "Cancer of unknown primary origin in the genomic era: Elucidating the dark box of cancer," Cancer Treat. Rev. **41**(7), 598–604 (2015).
[38]G. Viale *et al.*, "Comparative evaluation of an extensive histopathologic examination and a real-time reverse-transcription-polymerase chain reaction assay for mammaglobin and cytokeratin 19 on axillary sentinel lymph nodes of breast carcinoma patients," Ann. Surg. **247**(1), 136–142 (2008).
[39]I. Veys *et al.*, "Eighteen months clinical experience with the GeneSearch breast lymph node assay," Am. J. Surg. **198**(2), 203–209 (2009).
[40]C. S. Fisher *et al.*, "Molecular detection of micrometastatic breast cancer in histopathology—Negative axillary lymph nodes fails to predict breast cancer recurrence: A final analysis of a prospective multi-institutional cohort study," Ann. Surg. Oncol. **17**(3), 312–320 (2010).
[41]S. Gilad *et al.*, "Classification of the four main types of lung cancer using a microRNA-based diagnostic assay," J. Mol. Diagnos. **14**(5), 510–517 (2012).
[42]S. Liang *et al.*, in *International Thyroid Congress, American Thyroid Association, Mary Ann Liebert, Inc., 140 Huguenot Street, 3rd Floor New Rochelle, NY 10801, USA* (2015), pp. 356–A-383.
[43]Y. Spector *et al.*, "Development and validation of a microRNA-based diagnostic assay for classification of renal cell carcinomas," Mol. Oncol. **7**(3), 732–738 (2013).
[44]T. Nielsen *et al.*, "Analytical validation of the PAM50-based prosigna breast cancer prognostic gene signature assay and nCounter analysis system using formalin-fixed paraffin-embedded breast tumor specimens," BMC Cancer **14**, 177-2407-14-177 (2014).
[45]M. H. Veldman-Jones *et al.*, "Evaluating robustness and sensitivity of the nanostring technologies ncounter platform to enable multiplexed gene expression analysis of clinical samples," Cancer Res. **75**(13), 2587–2593 (2015).
[46]L. N. Harris *et al.*, "Use of biomarkers to guide decisions on adjuvant systemic therapy for women with early-stage invasive breast cancer: American society of clinical oncology clinical practice guideline," J. Clin. Oncol. **34**(10), 1134–1150 (2016).
[47]P. Wang *et al.*, "Absolute quantification of lung cancer related microRNA by droplet digital PCR," Biosens. Bioelectron. **74**, 836–842 (2015).
[48]U. Bissels *et al.*, "Absolute quantification of microRNAs by using a universal reference," RNA **15**(12), 2375–2384 (2009).
[49]E. L. van Dijk *et al.*, "Ten years of next-generation sequencing technology," Trends Genet. **30**(9), 418–426 (2014).
[50]B. T. Dickinson *et al.*, "Molecular markers for colorectal cancer screening," GUT, gutjnl-2014-308075, 2015.
[51]B. N. Hellquist *et al.*, "Effectiveness of population-based service screening with mammography for women ages 40 to 49 years with a high or low risk of breast cancer: Socioeconomic status, parity, and age at birth of first child," Cancer **121**(2), 251–258 (2015).
[52]S. M. Carter *et al.*, "Screening for cervical, prostate, and breast cancer: Interpreting the evidence," Am. J. Prev. Med. **49**(2), 274–285 (2015).
[53]N. G. Campos *et al.*, "Cervical cancer screening in low-resource settings: A cost-effectiveness framework for valuing tradeoffs between test performance and program coverage," Int. J. Cancer **137**(9), 2208–2219 (2015).
[54]R. S. Bresalier, S. Kopetz, and D. E. Brenner, "Blood-based tests for colorectal cancer screening: Do they threaten the survival of the FIT test?" Dig. Dis. Sci. **60**(3), 664–671 (2015).
[55]U. Menon, M. Griffin, and A. Gentry-Maharaj, "Ovarian cancer screening—Current status, future directions," Gynecol. Oncol. **132**(2), 490–495 (2014).
[56]M. Dufva, J. Petersen, and L. Poulsen, "Increasing the specificity and function of DNA microarrays by processing arrays at different stringencies," Anal. Bioanal. Chem. **395**(3), 669–677 (2009).
[57]S. Tam *et al.*, "Robust global microRNA expression profiling using next-generation sequencing technologies," Lab. Invest. **94**(3), 350–358 (2014).
[58]*Human Papillomavirus (HPV)-Associated Oropharyngeal Cancer*, edited by D. L. Miller and M. Sharon Stack (Springer International Publishing, Switzerland, 2015), pp. 314.

[59]M. Monleau *et al.*, "Comparison of different extraction techniques to profile microRNAs from human sera and peripheral blood mononuclear cells," BMC Genomics **15**, 395-2164-15-395 (2014).
[60]G. Di Leva and C. M. Croce, "miRNA profiling of cancer," Curr. Opin. Genet. Dev. **23**(1), 3–11 (2013).
[61]A. Hammerle-Fickinger *et al.*, "Validation of extraction methods for total RNA and miRNA from bovine blood prior to quantitative gene expression analyses," Biotechnol. Lett. **32**(1), 35–44 (2010).
[62]Z. Jiang *et al.*, "Isolation of RNA from equine peripheral blood cells: comparison of methods," Springerplus **2**, 478-1801-2-478 (2013).
[63]M. Eikmans *et al.*, "Blood cell mRNAs and microRNAs: Optimized protocols for extraction and preservation," Blood **121**(11), e81–e89 (2013).
[64]M. A. McAlexander, M. J. Phillips, and K. W. Witwer, "Comparison of methods for miRNA extraction from plasma and quantitative recovery of RNA from cerebrospinal fluid," Front. Genet. **4**, 83 (2013).
[65]A. Zampetaki and M. Mayr, "Analytical challenges and technical limitations in assessing circulating miRNAs," Thromb. Haemost. **108**(4), 592 (2012).
[66]J. S. McDonald *et al.*, "Analysis of circulating microRNA: Preanalytical and analytical challenges," Clin. Chem. **57**(6), 833–840 (2011).
[67]M. Eldh *et al.*, "Importance of RNA isolation methods for analysis of exosomal RNA: Evaluation of different methods," Mol. Immunol. **50**(4), 278–286 (2012).
[68]K. W. Witwer *et al.*, "Standardization of sample collection, isolation and analysis methods in extracellular vesicle research," J. Extracell. Vesicles **2**, 20360 (2013).
[69]M. Lucrecia Alvarez *et al.*, "Comparison of protein, microRNA, and mRNA yields using different methods of urinary exosome isolation for the discovery of kidney disease biomarkers," Kidney Int. **82**(9), 1024–1032 (2012).
[70]M. Doleshal *et al.*, "Evaluation and validation of total RNA extraction methods for microRNA expression analyses in formalin-fixed, paraffin-embedded tissues," J. Mol. Diagn. **10**(3), 203–211 (2008).
[71]I. Vomelova, Z. Vaníčková, and A. Šedo, "Methods of RNA Purification. All Ways (Should) Lead to Rome," Folia Biologica (Praha) **55**, 243–251 (2009).
[72]J. Shingara *et al.*, "An optimized isolation and labeling platform for accurate microRNA expression profiling," RNA **11**(9), 1461–1470 (2005).
[73]A. Podolska *et al.*, "How the RNA isolation method can affect microRNA microarray results," Acta Biochim. Pol. **58**, 535–540 (2011).
[74]N. Redshaw *et al.*, "A comparison of miRNA isolation and RT-qPCR technologies and their effects on quantification accuracy and repeatability," BioTechniques **54**(3), 155–164 (2013).
[75]X. Li, M. Mauro, and Z. Williams, "Comparison of plasma extracellular RNA isolation kits reveals kit-dependent biases," BioTechniques **59**(1), 13–17 (2015).
[76]B. Fromm, P. D. Harris, and L. Bachmann, "MicroRNA preparations from individual monogenean gyrodactylus salaris-a comparison of six commercially available totalRNA extraction kits," BMC Res. Notes **4**, 217-0500-4-217 (2011).
[77]P. A. Maroney *et al.*, "Direct detection of small RNAs using splinted ligation," Nat. Protocols **3**(2), 279–287 (2008).
[78]M. Hafner *et al.*, "RNA-ligase-dependent biases in miRNA representation in deep-sequenced small RNA cDNA libraries," RNA **17**(9), 1697–1712 (2011).
[79]C. A. Raabe *et al.*, "Biases in small RNA deep sequencing data," Nucleic Acids Res. **42**(3), 1414–1426 (2014).
[80]P. J. Mishra and R. Humeniuk, "MicroRNA polymorphisms," in *eLS* (John Wiley & Sons, Ltd, 2001).
[81]D. Leshkowitz *et al.*, "Differences in microRNA detection levels are technology and sequence dependent," RNA **19**(4), 527–538 (2013).
[82]J. Dabney and M. Meyer, "Length and GC-biases during sequencing library amplification: A comparison of various polymerase-buffer systems with ancient and modern DNA sequencing libraries," BioTechniques **52**(2), 87–94 (2012).
[83]D. Aird *et al.*, "Analyzing and minimizing PCR amplification bias in Illumina sequencing libraries," Genome Biol. **12**(2), R18 (2011).
[84]W. R. Swindell *et al.*, "Integrative RNA-seq and microarray data analysis reveals GC content and gene length biases in the psoriasis transcriptome," Physiol. Genomics **46**(15), 533–546 (2014).
[85]N. M. Alajez *et al.*, "MiR-218 suppresses nasopharyngeal cancer progression through downregulation of survivin and the SLIT2-ROBO1 pathway," Cancer Res. **71**(6), 2381–2391 (2011).
[86]M. Latreille *et al.*, "miR-375 gene dosage in pancreatic β-cells: implications for regulation of β-cell mass and biomarker development," J. Mol. Med. **93**(10), 1159–1169 (2015).
[87]M. Lundegard, K. Nylander, and K. Danielsson, "Difficulties detecting miRNA-203 in human whole saliva by the use of PCR," Med. Oral Patol. Oral Cir. Bucal **20**(2), e130–e134 (2015).
[88]P. Laudanski *et al.*, "Profiling of selected microRNAs in proliferative eutopic endometrium of women with ovarian endometriosis," Bio. Med. Res. Int. **2015**, 760698.
[89]C. Tian, Z. Zuo, and J.-L. Qiu, "Identification and characterization of ABA-responsive microRNAs in rice," J. Genet. Genomics **42**(7), 393–402 (2015).
[90]Y. Wu *et al.*, "Detection of extracellular RNAs in cancer and viral infection via tethered cationic lipoplex nanoparticles containing molecular beacons," Anal. Chem. **85**(23), 11265–11274 (2013).
[91]H. J. Peltier and G. J. Latham, "Normalization of microRNA expression levels in quantitative RT-PCR assays: identification of suitable reference RNA targets in normal and cancerous human solid tissues," RNA **14**(5), 844–852 (2008).
[92]J. M. Lee and Y. Jung, "Two-temperature hybridization for microarray detection of label-free MicroRNAs with attomole detection and superior specificity," Angew. Chem. Int. Ed. **50**(52), 12487–12490 (2011).
[93]A. A. Hardikar, R. J. Farr, and M. V. Joglekar, "Circulating microRNAs: understanding the limits for quantitative measurement by real-time PCR," J. Am. Heart Assoc. **3**(1), e000792 (2014).
[94]S. Das *et al.*, "Detection and serotyping of dengue virus in serum samples by multiplex reverse transcriptase PCR-ligase detection reaction assay," J. Clin. Microbiol. **46**(10), 3276–3284 (2008).
[95]J. J. Waggoner *et al.*, "Single-reaction, multiplex, real-time RT-PCR for the detection, quantitation, and serotyping of dengue viruses," PLoS Negl. Trop. Dis. **7**(4), e2116 (2013).

[96]R. Strassl *et al.*, "Real-time PCR assays for the quantification of HCV RNA: Concordance, discrepancies and implications for response guided therapy," PloS One **10**(8), e0135963 (2015).
[97]S. Bustin and R. Mueller, "Real-time reverse transcription PCR (qRT-PCR) and its potential use in clinical diagnosis," Clin. Sci. **109**, 365–379 (2005).
[98]J. Ma *et al.*, "Quantification of plasma miRNAs by digital PCR for cancer diagnosis," Biomarker Insights **8**, 127 (2013).
[99]N. Li *et al.*, "Digital PCR quantification of miRNAs in sputum for diagnosis of lung cancer," J. Cancer Res. Clin. Oncol. **140**(1), 145–150 (2014).
[100]C. W. Wei *et al.*, "Using a microfluidic device for 1 microl DNA microarray hybridization in 500 s," Nucleic Acids Res. **33**(8), e78 (2005).
[101]E. C. Hayden, "The $1,000 genome," Nature **507**(7492), 294–295 (2014).
[102]C. M. Hindson *et al.*, "Absolute quantification by droplet digital PCR versus analog real-time PCR," Nat. Methods **10**(10), 1003–1005 (2013).
[103]J. F. Huggett, S. Cowen, and C. A. Foy, "Considerations for digital PCR as an accurate molecular diagnostic tool," Clin. Chem. **61**(1), 79–88 (2015).
[104]E. Day, P. H. Dear, and F. McCaughan, "Digital PCR strategies in the development and analysis of molecular biomarkers for personalized medicine," Methods **59**(1), 101–107 (2013).
[105]S. C. Chapin and P. S. Doyle, "Ultrasensitive multiplexed microRNA quantification on encoded gel microparticles using rolling circle amplification," Anal. Chem. **83**(18), 7179–7185 (2011).
[106]J. M. Goldman *et al.*, "High affinity γPNA sandwich hybridization assay for rapid detection of short nucleic acid targets with single mismatch discrimination," Biomacromolecules **14**(7), 2253–2261 (2013).
[107]D. W. Wegman and S. N. Krylov, "Direct quantitative analysis of multiple miRNAs (DQAMmiR)," Angew. Chem. Int. Ed. **50**(44), 10335–10339 (2011).
[108]R. M. Graybill and R. C. Bailey, "Emerging biosensing approaches for microRNA analysis," Anal. Chem. **88**(1), 431–450 (2016).
[109]B. N. Johnson and R. Mutharasan, "Biosensor-based microRNA detection: techniques, design, performance, and challenges," Analyst **139**(7), 1576–1588 (2014).
[110]H.-C. Chang, G. Yossifon, and E. A. Demekhin, "Nanoscale electrokinetics and microvortices: How microhydrodynamics affects nanofluidic ion flux," Annu. Rev. Fluid Mech. **44**, 401–426 (2012).
[111]Z. Slouka, S. Senapati, and H.-C. Chang, "Microfluidic Systems with Ion-Selective Membranes," Annu. Rev. Anal. Chem. **7**(1), 317–335 (2014).
[112]W. Thormann, "Principles of isotachophoresis and dynamics of the isotachophoretic separation of two components," Sep. Sci. Technol. **19**(8–9), 455–467 (1984).
[113]I.-F. Cheng *et al.*, "A rapid field-use assay for mismatch number and location of hybridized DNAs," Lab Chip **10**(7), 828–831 (2010).
[114]Z. Slouka *et al.*, "Charge inversion, water splitting and vortex suppression due to DNA sorption on ion selective membranes and their ion current signatures," Langmuir **29**(26), 8275–8283 (2013).
[115]S. Basuray *et al.*, "Shear and AC field enhanced carbon nanotube impedance assay for rapid, sensitive, and mismatch-discriminating DNA hybridization," ACS Nano **3**(7), 1823–1830 (2009).
[116]S. Wang, H.-C. Chang, and Y. Zhu, "Hysteretic conformational transition of single flexible polyelectrolyte under resonant ac electric polarization," Macromolecules **43**(18), 7402–7405 (2010).
[117]P.-Y. Hsiao, Y.-F. Wei, and H.-C. Chang, "Unfolding collapsed polyelectrolytes in alternating-current electric fields," Soft Matter **7**(3), 1207–1213 (2011).
[118]S. Senapati *et al.*, "An ion-exchange nanomembrane sensor for detection of nucleic acids using a surface charge inversion phenomenon," Biosens. Bioelectron. **60**, 92–100 (2014).
[119]D. Taller *et al.*, "On-chip surface acoustic wave lysis and ion-exchange nanomembrane detection of exosomal RNA for pancreatic cancer study and diagnosis," Lab Chip **15**(7), 1656–1666 (2015).
[120]L.-J. Cheng and H.-C. Chang, "Microscale pH regulation by splitting water," Biomicrofluidics **5**(4), 046502 (2011).
[121]L.-J. Cheng and H.-C. Chang, "Switchable pH actuators and 3D integrated salt bridges as new strategies for reconfigurable microfluidic free-flow electrophoretic separation," Lab Chip **14**(5), 979 (2014).
[122]D. T. Conroy *et al.*, "Nonequilibrium hysteresis and Wien effect water dissociation at a bipolar membrane," Phys. Rev. E **86**(5), 056104 (2012).
[123]V. R. Minciacchi, M. R. Freeman, and D. Di Vizio, in *Seminars in Cell and Developmental Biology* (Elsevier, 2015), pp. 41–51.
[124]A. V. Vlassov *et al.*, "Exosomes: Current knowledge of their composition, biological functions, and diagnostic and therapeutic potentials," Biochim. Biophys. Acta (BBA)-Gen. Sub. **1820**(7), 940–948 (2012).
[125]A. Liga *et al.*, "Exosome isolation: A microfluidic road-map," Lab Chip **15**(11), 2388–2394 (2015).
[126]B. M. Venkatesan and R. Bashir, "Nanopore sensors for nucleic acid analysis," Nat. Nanotechnol. **6**(10), 615–624 (2011).
[127]Y. Wang *et al.*, "Nanopore-based detection of circulating microRNAs in lung cancer patients," Nat. Nanotechnol. **6**(10), 668–674 (2011).
[128]K. Tian *et al.*, "Designing a polycationic probe for simultaneous enrichment and detection of micrornas in a nanopore," ACS Nano **7**(5), 3962–3969 (2013).
[129]X. Zhang *et al.*, "Programming nanopore ion flow for encoded multiplex microRNA detection," ACS Nano **8**(4), 3444–3450 (2014).
[130]W. Li *et al.*, "Single protein molecule detection by glass nanopores," ACS Nano **7**(5), 4129–4134 (2013).
[131]Z. S. Siwy and S. Howorka, "Engineered voltage-responsive nanopores," Chem. Soc. Rev. **39**(3), 1115–1132 (2010).
[132]L.-Q. Gu and Y. Wang, "Nanopore single-molecule detection of circulating microRNAs," in *Circulating MicroRNAs* (Springer, 2013), pp. 255–268.
[133]G. Nguyen, S. Howorka, and Z. S. Siwy, "DNA strands attached inside single conical nanopores: ionic pore characteristics and insight into DNA biophysics," J. Membr. Biol. **239**(1–2), 105–113 (2011).
[134]Y. Yan *et al.*, "Ion current rectification inversion in conic nanopores: Nonequilibrium ion transport biased by ion selectivity and spatial asymmetry," J. Chem. Phys. **138**, 044706 (2013).

[135]Y. Yan *et al.*, "Energy conversion efficiency of nanofluidic batteries: Hydrodynamic slip and access resistance," J. Phys. Chem. C **117**(16), 8050–8061 (2013).
[136]S. Liu *et al.*, "Plasmonic hotspots of dynamically assembled nanoparticles in nanocapillaries: Towards a micro ribonucleic acid profiling platform," Biomicrofluidics **7**(6), 061102 (2013).
[137]V. V. Thacker *et al.*, "Studying DNA translocation in nanocapillaries using single molecule fluorescence," Appl. Phys. Lett. **101**(22), 223704 (2012).
[138]K. Healy, B. Schiedt, and A. P. Morrison, "Solid-state nanopore technologies for nanopore-based DNA analysis," Nanomedicine (Lond.) **2**(6), 875–897 (2007).
[139]R. S. Kuczenski, H.-C. Chang, and A. Revzin, "Dielectrophoretic microfluidic device for the continuous sorting of Escherichia coli from blood cells," Biomicrofluidics **5**, 032005 (2011).
[140]I.-F. Cheng *et al.*, "A continuous high-throughput bioparticle sorter based on 3D traveling-wave dielectrophoresis," Lab Chip **9**(22), 3193–3201 (2009).
[141]D. Hou, S. Maheshwari, and H.-C. Chang, "Rapid bioparticle concentration and detection by combining a discharge driven vortex with surface enhanced Raman scattering," Biomicrofluidics **1**, 014106 (2007).
[142]S. K. Thamida and H.-C. Chang, "Nonlinear electrokinetic ejection and entrainment due to polarization at nearly insulated wedges," Phys. Fluids **14**, 4315 (2002).
[143]M. Fujita *et al.*, "Structural study on gold nanoparticle functionalized with DNA and its non-cross-linking aggregation," J. Colloid Interface Sci. **368**(1), 629–635 (2012).
[144]S. Maheshwari *et al.*, "Coupling between precipitation and contact-line dynamics: Multiring stains and stick-slip motion," Phys. Rev. Lett. **100**(4), 044503 (2008).
[145]S. Basuray and H.-C. Chang, "Induced dipoles and dielectrophoresis of nanocolloids in electrolytes," Phys. Rev. E **75**(6), 060501 (2007).
[146]Z. Chen *et al.*, "Capture and release of viruses using amino-functionalized silica particles," Anal. Chim. Acta **569**(1), 76–82 (2006).
[147]N. Chetwani *et al.*, "High-frequency AC electrospray ionization source for mass spectrometry of biomolecules," J. Am. Soc. Mass Spectrom. **21**(11), 1852–1856 (2010).
[148]N. Chetwani *et al.*, "Frequency dependence of alternating current electrospray ionization mass spectrometry," Anal. Chem. **83**(8), 3017–3023 (2011).
[149]J. Ho *et al.*, "Paper-based microfluidic surface acoustic wave sample delivery and ionization source for rapid and sensitive ambient mass spectrometry," Anal. Chem. **83**(9), 3260–3266 (2011).
[150]Y. Wang *et al.*, "Electrospray cone-jet breakup and droplet production for electrolyte solutions," EPL **99**(6), 64003 (2012).
[151]D. Taller, D. B. Go, and H.-C. Chang, "Self-similar micron-size and nanosize drops of liquid generated by surface acoustic waves," Phys. Rev. Lett. **109**(22), 224301 (2012).
[152]F. Plouraboué and H.-C. Chang, "Symmetry breaking and electrostatic attraction between two identical surfaces," Phys. Rev. E **79**(4), 041404 (2009).
[153]F. Xie *et al.*, "Preparation of rhombus-shaped micro/nanofluidic channels with dimensions ranging from hundred nanometers to several micrometers," J. Nanosci. Nanotechnol. **10**(11), 7277–7281 (2010).
[154]G. Yossifon *et al.*, "Nonlinear current-voltage characteristics of nanochannels," Phys. Rev. E **79**(4), 046305 (2009).
[155]G. Yossifon and H.-C. Chang, "Selection of nonequilibrium overlimiting currents: universal depletion layer formation dynamics and vortex instability," Phys. Rev. Lett. **101**(25), 254501 (2008).
[156]G. Yossifon, Y.-C. Chang, and H.-C. Chang, "Rectification, gating voltage, and interchannel communication of nanoslot arrays due to asymmetric entrance space charge polarization," Phys. Rev. Lett. **103**(15), 154502 (2009).
[157]G. Yossifon *et al.*, "Eliminating the limiting-current phenomenon by geometric field focusing into nanopores and nanoslots," Phys. Rev. E **81**(4), 046301 (2010).
[158]G. Yossifon and H.-C. Chang, "Changing nanoslot ion flux with a dynamic nanocolloid ion-selective filter: Secondary overlimiting currents due to nanocolloid-nanoslot interaction," Phys. Rev. E **81**(6), 066317 (2010).
[159]G. Yossifon, P. Mushenheim, and H.-C. Chang, "Controlling nanoslot overlimiting current with the depth of a connecting microchamber," EPL **90**(6), 64004 (2010).
[160]F. Mavré *et al.*, "Bipolar electrodes: A useful tool for concentration, separation, and detection of analytes in microelectrochemical systems," Anal. Chem. **82**(21), 8766–8774 (2010).
[161]Y. Tu *et al.*, "Fluorescence quenching of gold nanoparticles integrating with a conformation-switched hairpin oligonucleotide probe for microRNA detection," Chem. Commun. **48**(87), 10718–10720 (2012).
[162]A. Bek *et al.*, "Fluorescence enhancement in hot spots of AFM-designed gold nanoparticle sandwiches," Nano Lett. **8**(2), 485–490 (2008).
[163]M. Ringler *et al.*, "Shaping emission spectra of fluorescent molecules with single plasmonic nanoresonators," Phys. Rev. Lett. **100**(20), 203002 (2008).
[164]C. M. Galloway, P. G. Etchegoin, and E. C. Le Ru, "Ultrafast nonradiative decay rates on metallic surfaces by comparing surface-enhanced Raman and fluorescence signals of single molecules," Phys. Rev. Lett. **103**(6), 063003 (2009).
[165]Y. Chen, K. Munechika, and D. S. Ginger, "Dependence of fluorescence intensity on the spectral overlap between fluorophores and plasmon resonant single silver nanoparticles," Nano Lett. **7**(3), 690–696 (2007).
[166]F. Tam *et al.*, "Plasmonic enhancement of molecular fluorescence," Nano Lett. **7**(2), 496–501 (2007).
[167]R. Gill and E. C. Le Ru, "Fluorescence enhancement at hot-spots: The case of Ag nanoparticle aggregates," Phys. Chem. Chem. Phys. **13**(36), 16366–16372 (2011).
[168]R. G. Sosnowski *et al.*, "Rapid determination of single base mismatch mutations in DNA hybrids by direct electric field control," Proc. Natl. Acad. Sci. U.S.A. **94**(4), 1119–1123 (1997).
[169]T. Strunz *et al.*, "Dynamic force spectroscopy of single DNA molecules," Proc. Natl. Acad. Sci. **96**(20), 11277–11282 (1999).
[170]J. Schiffbauer, S. Park, and G. Yossifon, "Electrical impedance spectroscopy of microchannel-nanochannel interface devices," Phys. Rev. Lett. **110**(20), 204504 (2013).

[171]J. Feng *et al.*, "Impedance characteristics of amine modified single glass nanopores," Anal. Chem. **82**(11), 4520–4528 (2010).
[172]N. Chetwani, S. Maheshwari, and H.-C. Chang, "Universal cone angle of ac electrosprays due to net charge entrainment," Phys. Rev. Lett. **101**(20), 204501 (2008).
[173]C.-M. Wang *et al.*, "Surface engineering of synthetic nanopores by atomic layer deposition and their applications," Front. Mater. Sci. **7**(4), 335–349 (2013).
[174]P. Rao, E. Benito, and A. Fischer, "MicroRNAs as biomarkers for CNS disease," Front. Mol. Neurosci. **6**, 39 (2013).
[175]G. Nagashima *et al.*, "Superheating and homogeneous single bubble nucleation in a solid-state nanopore," Phys. Rev. Lett. **113**(2), 024506 (2014).
[176]Y. Wang *et al.*, "Diffraction-limited ultrasensitive molecular nano-arrays with singular nano-cone scattering," Biomicrofluidics **8**(2), 021101 (2014).
[177]Y. Wang *et al.*, "Nano-cone optical fiber array sensors for MiRNA profiling," in *SPIE Proceedings, Biosensing and Nanomedicine VI* (International Society for Optics and Photonics, San Diego, California, United States, 2013), pp. 88120Q-6.
[178]Y. Wang, F. Plouraboue, and H.-C. Chang, "Broadband converging plasmon resonance at a conical nanotip," Opt. Express **21**(5), 6609–6617 (2013).
[179]Y. Wang and H.-C. Chang, "Surface plasmon polaritons: Geometric resonance at singularities," in *Proceedings of the American Physical Society March Meeting* (APS, Dallas, Texas, 2011), pp. BAPS.2011.MAR.A32.12.
[180]S. Marczak *et al.*, "Induced nanoparticle aggregation for short nucleic acid quantification by depletion isotachophoresis," Anal. Chem. (submitted).
[181]P. F. O'Neill *et al.*, "Advances in three-dimensional rapid prototyping of microfluidic devices for biological applications," Biomicrofluidics **8**(5), 052112 (2014).
[182]Z. Slouka *et al.*, "Integrated, DC voltage-driven nucleic acid diagnostic platform for real sample analysis: Detection of oral cancer," Talanta **145**, 35–42 (2015).
[183]C. Wang *et al.*, "Atomic layer deposition modified track-etched conical nanochannels for protein sensing," Anal. Chem. **87**(16), 8227–8233 (2015).